Dual-Porosity Models for Flow in Naturally Fractured Reservoirs*

Jim Douglas, Jr.,†
and
Todd Arbogast†

Purdue University

Technical Report # 95 / April 1989

Published in Dynamics of Fluids in Hierarchical Porous Media,
J. H. Cushman, ed., Academic Press, London, 1990, pp. 177–221.

*This work was supported in part by the National Science Foundation.
†Department of Mathematics, Purdue University, West Lafayette, Indiana 47907.

§1. Introduction

1.1. Naturally fractured reservoirs.

Within a naturally fractured reservoir there is an interconnected system of fracture planes dividing the porous rock, which will be called the *matrix*, into a collection of blocks. This is somewhat of an idealization, but it is sufficient for the simulation of naturally fractured reservoirs. The fractures, while very thin, have a profound effect on the flow of fluids within the reservoir. Most of the fluid resides in the matrix, where it moves very slowly. When fluid reaches the surface of a matrix block and enters the fractures, it flows comparatively quickly, since the fractures form paths of high permeability. Thus, a naturally fractured reservoir has not two but *three* important scales of length. The smallest scale, on the order of millimeters, is that of the pores. The intermediate and new scale is that of the fracture spacing, which is on the order of meters. Finally, the reservoir length is on the order of kilometers.

In any practical spatial discretization of the reservoir, there will be at least a few matrix blocks in every grid cell and usually many. We cannot and, fortunately, we need not compute the flow of fluids within the individual fractures. We consider dual-porosity models which enable us to simulate the flow in naturally fractured reservoirs in a fashion that is both computationally tractable and sufficiently precise for practical purposes.

We begin by recalling some ideas related to single porosity models.

1.2. A single porosity model.

In a porous medium, define the rock properties porosity and permeability at each point, as usual, as the pore void space per unit bulk volume and the coefficient in Darcy's law (see (2.1.2) below) describing the rock's resistance to flow, respectively; see [10], [14], [15], [25], and [30] as general references on porous media flow. A fractured reservoir could be modeled by allowing the porosity and permeability to vary rapidly and discontinuously over the reservoir; both of these quantities are dramatically greater in the fractures than in the porous rock. However, the computational and data requirements of treating such a model would be too great to approximate the flow in the entire reservoir, and this model must be rejected for practical simulation.

1.3. A dual-porosity model.

As an alternative, one might try to avoid the discontinuous nature of the porosity and permeability by replacing them locally by their average values. While such a simulation could be done as in the unfractured case, the result would be unsatisfactory, in that correlation to physical observations would not be obtained. The interchange of fluid between the matrix and the fractures must be modeled. The usual technique, due to [26], [9], and [36], is described below.

It has been observed that naturally fractured reservoirs behave as if they possessed *two* porous structures rather than one [9], [26], [36]. The system of fractures is on a much finer

scale than the reservoir as a whole; hence, it can be viewed as a porous structure itself (see Figure 1). The fractures form the "void spaces" while the matrix blocks play the role of the "solid rock". Of course, there is a difference from the usual porous system: the "solid part" is in itself permeable.

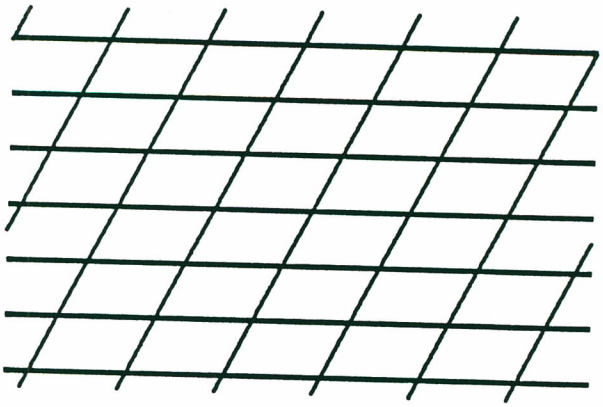

FIG. 1. Cross section of a naturally fractured porous medium, depicting the fracture planes.

On the finest scale, the matrix porous structure has a porosity ϕ and a (tensor) permeability $\mathbf{k}$ defined in the usual way, and they are on the order of a tenth and a few millidarcies to a darcy, respectively. On the scale of the fracture system, we can define a fracture porosity Φ as the fracture void space per unit bulk volume, so that Φ is quite small, perhaps on the order of a hundredth. We can also define a fracture permeability tensor $\mathbf{K}$ as the coefficient in the Darcy law that represents resistance to fluid flow *completely within the fracture system*; that is, $\mathbf{K}$ is defined by considering the matrix to be impermeable [9], [36]. It is quite large in magnitude, perhaps on the order of several darcies [22], [34], [36].

It is well known how to model the flow of fluids in a single porous structure; a dual-porosity model is much more complicated. The main conceptual difficulty lies in the fact that, since the fracture system is viewed as a porous medium, *both* matrix and fracture flow are defined at each point of the matrix. Consequently, we see fluid flow as a combination of general macroscopic motion over the reservoir and flow within matrix blocks, not as actual motion around the matrix blocks (Figure 2). Since flow in the fractures is much more rapid than in the matrix, we shall assume that fluid does not flow directly from one matrix block to another. Rather, it first flows into the fracture system, and then it can pass into another block or remain in the fractures. We shall determine whether any element of fluid belongs to the matrix or to the fractures by considering the reservoir to consist of two "sheets". One sheet, which we call Ω, contains the fracture flow. The matrix flow is on the other sheet, called Ω_m; we denote the ith matrix block by Ω_i and assume them to be disjoint, so that $\cup \Omega_i = \Omega_m \subset \Omega$. As a consequence of the assumption that fluid flows from the matrix into the fracture system and vice versa, fluid flows from one "sheet" to

the other. It is this matrix-fracture interaction on the scale of the fracture spacing that must be carefully modeled. Its effect on the fracture system will be averaged over the size of an individual matrix block, which is comparable to the fracture spacing; however, the interaction must be treated on a smaller scale as far as the matrix is concerned.

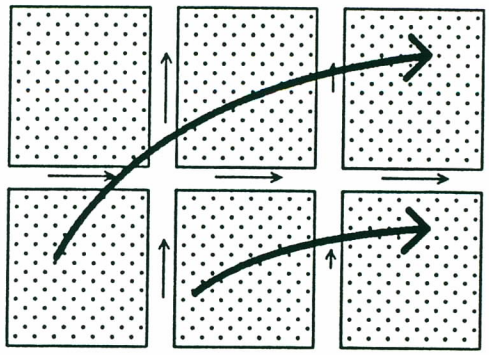

FIG. 2. The macroscopic fracture flow.

The equations that describe the flow in the fracture system will contain a source term that represents the flow of fluid from the matrix to the fractures; this term will be macroscopically distributed over the entire reservoir, as is the fracture flow itself. The definition of the term will be in terms of quantities that are on the scale of the matrix blocks.

The matrix equations will be effected on the scale of the fracture spacing. In particular, fluid flows into or out of an individual matrix block only through its surface. Such an interaction should be modeled as a boundary condition on the flow equation; fracture quantities will be used to define these boundary conditions.

1.4. Some remarks on the derivation of dual-porosity models.

The models presented in this paper will be derived first on the basis of physical intuition by applying the dual-porosity idea of the previous subsection to define the equations of flow and then by the mathematical theory of homogenization [11], [29]. This will give us both greater confidence that our physical intuition of the model is correct and a better understanding of the resulting model; in particular, we shall derive an explicit expression for the fracture system's permeability tensor $\mathbf{K}$. Homogenization will be used only in a formal sense herein; that is, a rigorous convergence argument will not be carried out.

1.5. A summary of the results.

In §2 we model single-phase flow of a liquid of constant compressibility in a naturally fractured reservoir intuitively by incorporating the physics of such flow into the dual-porosity concept. After giving some general background on homogenization theory, we rederive the model. There are some subtle differences in the models obtained through the two derivations, but none of any real practical concern. We conclude the section by

mentioning some of the mathematical properties of the model, including existence and uniqueness of the solution of the differential system.

In §3, we take up a study of the flow of two immiscible fluids, such as oil and water, under the assumption of incompressibility. Again, we first derive a model on physical grounds and then rederive it from homogenization. Actually, we present three models for immiscible flow, varying in physical and mathematical complexity and therefore in the amount of computational effort needed to approximate the solution of them.

We present in §4 some relatively simple finite difference discretization procedures in a computationally tractable form achieved by separating the matrix calculations from those of the fracture system. Both the single phase and immiscible cases are discussed. In §5 we present the results of some simulations of immiscible flow based on implementing the algorithms of the fourth section which compare and contrast the predictions of the three immiscible models and an unfractured reservoir model. Finally, in §6, we consider briefly some models generalizing those presented herein.

§2. Single Phase Flow

2.1. Introduction.

Consider the flow of a fluid of constant compressibility c in the reservoir; that is, a fluid that satisfies the equation of state

$$d\rho = c\rho\, dp, \tag{2.1.1}$$

where ρ is the density of the fluid and p is the pressure. Let μ be its viscosity. Since ρ is an exponential function of p, flow can be modeled in terms of either variable, but density is the more convenient choice. Let $\rho_f(x,t)$ denote the density of the fluid in the fracture system and $\rho_m(x,t)$ that in the matrix.

For expositional and computational convenience, we shall represent wells as external source terms of the form $q_{\text{ext}}(x,t)$; they could also be represented by a boundary condition.

The equations describing single phase flow in a single porosity system are well understood. Darcy's law relates the macroscopic Darcy velocity $v(x,t)$ to the pressure:

$$v = -\frac{\mathbf{k}}{\mu}(\nabla p - g\rho), \tag{2.1.2}$$

where g is the gravitational, downward-pointing, constant vector and where notation is simplified a bit by writing $\frac{1}{\mu}\mathbf{k}$ as $\frac{\mathbf{k}}{\mu}$. Conservation of mass states that

$$\phi\, \rho_t + \nabla \cdot (\rho v) = q_{\text{ext}}, \tag{2.1.3}$$

where the subscript t denotes partial differentiation with respect to time. Then, the equation of state (2.1.1) implies that

$$\phi\,\rho_t - \nabla\cdot\left[\frac{\mathbf{k}}{\mu c}(\nabla\rho - cg\rho^2)\right] = q_{\text{ext}}. \tag{2.1.4}$$

The first successful attempts at modeling single phase flow in naturally fractured reservoirs took place in the early 1960's [9], [36]; in each of these models a "quasi-steady state" assumption was made about the matrix-fracture interaction. Models that avoided this assumption were presented later [22], [34]; unfortunately, these new models were not truly of the dual-porosity type, so that they were difficult to manage computationally. Recently, a general form of the single phase model has appeared [5], [19]; it is this model that we consider below.

2.2. Modeling by physical arguments.

Equation (2.1.4) is the starting point for describing the flow in both the fracture and matrix systems, since each is considered to be a porous medium. As mentioned in the introduction, the equations for the fracture system require a macroscopically distributed matrix source term $q_m(x,t)$ to represent flow from the matrix to the fractures; it is defined below in (2.2.5). Hence, flow in the fractures is described by

$$\Phi\,\rho_{f,t} - \nabla\cdot\left[\frac{\mathbf{K}}{\mu c}(\nabla\rho_f - cg\rho_f^2)\right] = q_{\text{ext}} + q_m \quad \text{for} \quad x\in\Omega,\ t>0. \tag{2.2.1}$$

The matrix equations are not special. On each block Ω_i,

$$\phi\,\rho_{m,t} - \nabla\cdot\left[\frac{\mathbf{k}}{\mu c}(\nabla\rho_m - cg\rho_m^2)\right] = 0 \quad \text{for } x\in\Omega_i,\ t>0. \tag{2.2.2}$$

We have assumed that the wells interact only with the fracture system; this assumption is based on the fact that flow is much more rapid in the fracture system than in the matrix. Numerical experiments have shown that this assumption is reasonable [22].

Recall that the matrix sees the fractures only at the surfaces of the blocks. There, we must enforce continuity of pressure (or density) in some way. It is not immediately obvious how to do this, since the fracture system has been macroscopically averaged on a scale comparable to the size of the matrix blocks, but the flow in the fractures around an individual matrix block being much faster than the internal matrix flow allows us to assume that the fracture flow essentially reaches equilibrium with respect to the matrix flow. Then, at each time our boundary condition is that the matrix pressure is constant over the surface of the block; which pressure value to take in the differential model is not uniquely determined, though almost any reasonable choice will yield the same value in discrete form. It is mathematically convenient to take, for each i, the boundary condition

$$\rho_m(x,t) = \frac{1}{|\hat{\Omega}_i|}\int_{\hat{\Omega}_i}\rho_f(\xi,t)\,d\xi \quad \text{for } x\in\partial\Omega_i,\ t>0, \tag{2.2.3}$$

where $\hat{\Omega}_i$ is Ω_i together with half of the surrounding fractures, $|\hat{\Omega}_i|$ denotes the volume of $\hat{\Omega}_i$, and "∂" denotes the boundary of the set.

The matrix source term can be defined as follows. The total mass of fluid leaving the ith matrix block per unit time is

$$-\int_{\partial\Omega_i}\left[\frac{\mathbf{k}}{\mu c}(\nabla\rho_m - cg\rho_m^2)\right]\cdot\nu\,da(x),$$

where ν is the outer normal unit-vector to the surface. The divergence theorem then implies that

$$-\int_{\partial\Omega_i}\left[\frac{\mathbf{k}}{\mu c}(\nabla\rho_m - cg\rho_m^2)\right]\cdot\nu\,da(x)$$
$$=-\int_{\Omega_i}\nabla\cdot\left[\frac{\mathbf{k}}{\mu c}(\nabla\rho_m - cg\rho_m^2)\right]dx = -\int_{\Omega_i}\phi\,\rho_{m,t}\,dx,$$

where the last equality follows from (2.2.2). This fluid must be distributed into the fracture system in the vicinity of the block. Again, the exact way this is done will have little effect on the computations. It is reasonable to spread it out evenly over $\hat{\Omega}_i$; hence, let

$$q_{m,i}(t) = -\frac{1}{|\hat{\Omega}_i|}\int_{\Omega_i}\phi\rho_{m,t}(\xi,t)\,d\xi, \tag{2.2.4}$$

and let $\chi_i(x)$ be the characteristic function of $\hat{\Omega}_i$:

$$\chi_i(x) = \begin{cases} 1 & \text{for } x\in\hat{\Omega}_i,\\ 0 & \text{for } x\notin\hat{\Omega}_i.\end{cases}$$

Finally, let

$$q_m(x,t) = \sum_i q_{m,i}(t)\,\chi_i(x) \quad \text{for } x\in\Omega,\ t>0. \tag{2.2.5}$$

The model is completed by specifying an outer boundary condition and the initial densities. For example, we might assume that there is no flow across $\partial\Omega$. Then,

$$\left[\frac{\mathbf{K}}{\mu c}\left(\nabla\rho_f - cg\rho_f^2\right)\right]\cdot\nu = 0 \quad \text{for } x\in\partial\Omega,\ t>0. \tag{2.2.6}$$

Let the initial values be

$$\rho_f(x,0) = \rho_{\text{init},f}(x) \quad \text{for } x\in\Omega, \tag{2.2.7}$$

$$\rho_m(x,0) = \rho_{\text{init},m}(x) \quad \text{for } x\in\Omega_m. \tag{2.2.8}$$

Most likely,

$$\rho_{\text{init},m} = \frac{1}{|\hat{\Omega}_i|}\int_{\Omega_i}\rho_{\text{init},f}(\xi)\,d\xi \quad \text{for } x\in\Omega_i, \tag{2.2.9}$$

so that the fluids are in equilibrium initially. For consistency, assume that (2.2.3) and (2.2.6) hold for $t=0$.

2.3. A brief description of homogenization.

In order to rederive the model by homogenization let us recall some of the main ideas of this theory [11], [20], [29]. Suppose that we are given a physical system with a periodic fine structure. In theory, the governing equations, called the *microscopic* model, of that system can be derived from physics; however the model will capture far more detailed information than we care to know (or far more than we care to pay for in computation). Let us represent this schematically. If $\theta(x)$ is some quantity of physical relevance, it may have a graph such as that shown in Figure 3, with θ oscillating about some average value as it varies from point to point within the fine structure. It may suffice to know only this general trend (or "local average") of θ; homogenization is a mathematical procedure that seeks to derive an equation (or set of equations) for the general trend of θ by constructing a limit of the microscopic model as the period in the periodic structure tends to zero. These equations are then called the *macroscopic* model. Since this model is less detailed, it is usually the case that it is easier to approximate numerically than the original microscopic model for θ.

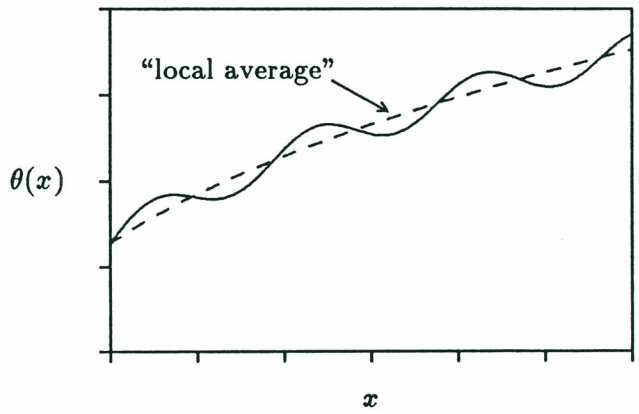

FIG. 3. The "local average" of a function θ.

2.4. Modeling by homogenization.

The model of §§2.2 will be rederived by homogenization, following [7]. Darcy's law is assumed to hold on the smallest (i.e., pore) scale. It is at the scale of the fracture spacing that the problem needs explanation.

Idealize the reservoir by assuming that the fractures form three sets of parallel, equally-spaced planes (see Figure 4), so that all matrix blocks are identical and the reservoir has a periodic structure. Let $\mathcal{Q}$ be a period, or *cell*, of this structure, containing a matrix block $\mathcal{Q}_m$ and half of the surrounding fractures $\mathcal{Q}_f$ (Figure 5). Each $\hat{\Omega}_i$ is then some translate of $\mathcal{Q}$.

The microscopic model, which for simplicity will be taken to have all physical parameters as constants, is given by a single porosity system with discontinuous porosity and permeability as described in §§1.2 above and contains all of the relevant physics, and it

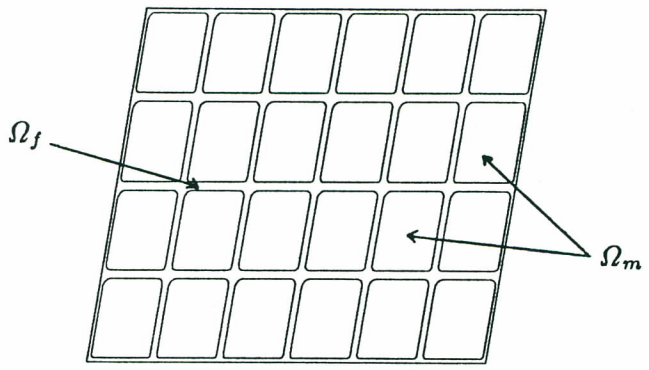

FIG. 4. The periodic reservoir Ω.

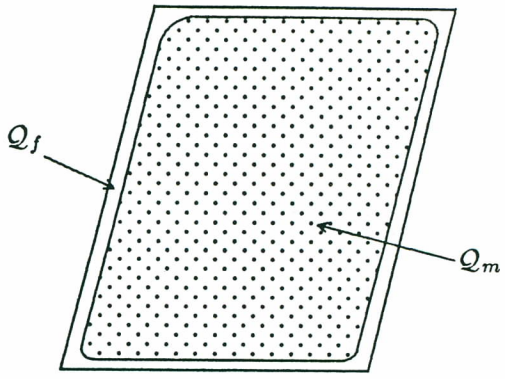

FIG. 5. The reservoir cell $\mathcal{Q}$.

does so without requiring any intuition about the dual-porosity concept. Let Φ^* be the "porosity" of an individual fracture; that is, the fracture porosity defined on a finer scale than the fracture width. It is a little less than one, since there is always rock detritus in the fracture. The permeability of an individual fracture is very large and should be a scalar, denoted by K^*; it is defined on the scale of the pores, not on the scale of the fracture spacing, as is $\mathbf{K}$. From §§2.1 above, (2.1.4) is posed over Ω; however, for clarity we write this on the two parts of the domain separately:

$$\Phi^* \rho_{f,t} - \nabla \cdot \left[\frac{K^*}{\mu c} (\nabla \rho_f - cg \rho_f^2) \right] = q_{\text{ext}} \quad \text{for } x \in \Omega_f, \ t > 0, \tag{2.4.1}$$

$$\phi \rho_{m,t} - \nabla \cdot \left[\frac{\mathbf{k}}{\mu c} (\nabla \rho_m - cg \rho_m^2) \right] = q_{\text{ext}} \quad \text{for } x \in \Omega_m, \ t > 0. \tag{2.4.2}$$

On the interface $\partial\Omega_m$ between the two domains, impose continuity of pressure (i.e., density) and continuity of mass flux between the two domains. Hence,

$$\rho_m = \rho_f \quad \text{for } x \in \partial\Omega_m, \ t > 0, \tag{2.4.3}$$

$$\left[\frac{K^*}{\mu c} (\nabla \rho_f - cg \rho_f^2) \right] \cdot \nu = \left[\frac{\mathbf{k}}{\mu c} (\nabla \rho_m - cg \rho_m^2) \right] \cdot \nu \quad \text{for } x \in \partial\Omega_m, \ t > 0. \tag{2.4.4}$$

The fine structure that must be homogenized is the nearly periodic behavior of the system on the scale of the fracture spacing. Since this behavior is irrelevant in the evaluation of the overall flow in the reservoir, we consider the limit as the matrix blocks become small. To quantify this shrinkage, let ϵ be a parameter such that $0 < \epsilon \leq 1$. When $\epsilon = 1$, we have the original microscopic model. For $\epsilon < 1$, we pose a fractured reservoir that is identical to the original one except that the fracture planes are assumed located at ϵ times the original distance apart. More explicitly, let the reservoir be composed of cells of size $\epsilon\mathcal{Q}$ (Figure 6), and embed the microscopic model ($\epsilon = 1$) into a family of models (for $\epsilon < 1$). To this end, for each ϵ, let Ω_m^ϵ be the matrix part of the reservoir and Ω_f^ϵ the fracture

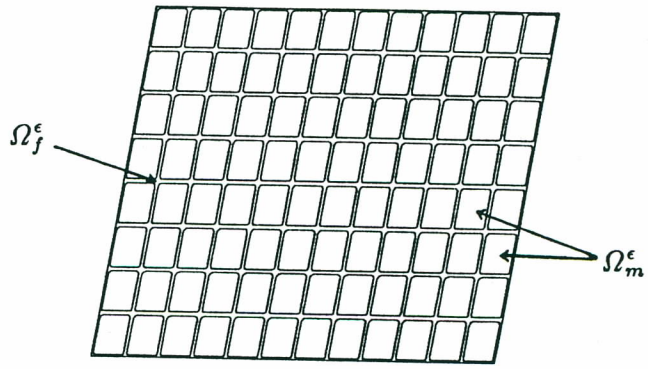

FIG. 6. The reservoir Ω^ϵ for $\epsilon = \frac{1}{2}$.

part. (Ignore the outer boundary of the reservoir; a rigorous homogenization could not, but the point here is to understand the flow in the interior of the reservoir, since (2.2.6) holds on the outer boundary.)

Then, (2.4.1)–(2.4.4) should hold, though it is necessary to scale the physical parameters in the equations in terms of ϵ, as can be seen in two different ways. First, if no scaling were done, the homogenization process would produce a single porosity model with averaged coefficients, which has already been pointed out to be inadequate. Second, proper scaling can in some sense preserve matrix-to-fracture mass flow as $\epsilon \to 0$. This mass flux is

$$\int_{\partial\Omega_m^\epsilon} \left[\frac{\mathbf{k}}{\mu c}(\nabla\rho_m - cg\,\rho_m^2)\right] \cdot \nu\, ds(x) = \int_{\Omega_m^\epsilon} \nabla \cdot \left[\frac{\mathbf{k}}{\mu c}(\nabla\rho_m - cg\,\rho_m^2)\right] dx.$$

On an individual ϵ-matrix block $\Omega_i = \epsilon\,\mathcal{Q}_m$, a change of variables shows that

$$\int_{\epsilon\mathcal{Q}_m} \nabla \cdot \left[\frac{\mathbf{k}}{\mu c}(\nabla\rho_m - cg\rho_m^2)\right] dx = \int_{\mathcal{Q}_m} \epsilon^{-1}\nabla \cdot \left[\frac{\mathbf{k}}{\mu c}(\epsilon^{-1}\nabla\rho_m - cg\,\rho_m^2)\right] \epsilon^3\, dx.$$

Adding these over the matrix blocks (ϵ-cells) leads to the total matrix-fracture flow

$$\sum_{\epsilon\text{-cells}} \int_{\mathcal{Q}_m} \epsilon^{-1}\,\nabla \cdot \left[\frac{\mathbf{k}}{\mu c}(\epsilon^{-1}\nabla\rho_m - cg\,\rho_m^2)\right] \epsilon^3\, dx.$$

(In the above the notation has been abused slightly; the ϵ-cells should have been translated over the reservoir). Since there are on the order of ϵ^{-3} cells in Ω_m^ϵ, this quantity will diverge as $\epsilon \to 0$ unless $\mathbf{k}$ is scaled by ϵ^2. It also appears that gravity should be compensated by ϵ^{-1}, though this is not essential.

This scaling has the effect of making the matrix progressively less permeable as $\epsilon \to 0$. However, the blocks being smaller implies that more of the fluid in the block is near the surface, so that the scaling prevents the model from reducing the time needed for fluid

within the matrix to reach the fractures (as $\epsilon \to 0$). This is the crucial physical process that must be modeled carefully.

Thus, modulo scale factors, each of the ϵ-models is identical to that in (2.4.1)–(2.4.4) above. To avoid confusion as to the value of ϵ, let ρ_f^ϵ and ρ_m^ϵ denote the solution to the ϵ-model:

$$\Phi^* \rho^\epsilon_{f,t} - \nabla \cdot \left[\frac{K^*}{\mu c} \left(\nabla \rho_f^\epsilon - c g(\rho_f^\epsilon)^2 \right) \right] = q_{\text{ext}} \quad \text{for } x \in \Omega_f^\epsilon,\ t > 0, \tag{2.4.1/ϵ}$$

$$\phi \rho^\epsilon_{m,t} - \nabla \cdot \left[\frac{\epsilon^2 \mathbf{k}}{\mu c} \left(\nabla \rho_m^\epsilon - \epsilon^{-1} c g(\rho_m^\epsilon)^2 \right) \right] = q_{\text{ext}} \quad \text{for } x \in \Omega_m^\epsilon,\ t > 0, \tag{2.4.2/ϵ}$$

$$\rho_m^\epsilon = \rho_f^\epsilon \quad \text{for } x \in \partial\Omega_m^\epsilon,\ t > 0, \tag{2.4.3/ϵ}$$

$$\left[\frac{K^*}{\mu c} \left(\nabla \rho_f^\epsilon - c g(\rho_f^\epsilon)^2 \right) \right] \cdot \nu = \left[\frac{\epsilon^2 \mathbf{k}}{\mu c} \left(\nabla \rho_m^\epsilon - \epsilon^{-1} c g(\rho_m^\epsilon)^2 \right) \right] \cdot \nu \quad \text{for } x \in \partial\Omega_m^\epsilon,\ t > 0. \tag{2.4.4/ϵ}$$

We now perform homogenization heuristically. Assume that any point is described by two variables: $x \in \Omega$ giving the general location of the point and $y \in \mathcal{Q}$ the location of the point within the ϵ-cell $\epsilon\mathcal{Q}$. Clearly, x and y are related by the scale ϵ:

$$\epsilon y \sim x$$

(up to translation). As a consequence, the gradient operator becomes

$$\nabla \sim \frac{1}{\epsilon} \nabla_y + \nabla_x, \tag{2.4.5}$$

with ∇_y and ∇_x being the gradient operators with respect to y and x, respectively.

Assume that the solution behaves as if it were a function of these two space variables (and time) and that it can be expanded in a power series in the scale parameter ϵ; that is, assume that the oscillations in the solution have wavelengths given by powers of ϵ. Hence,

$$\rho_f^\epsilon(x,t) \sim \sum_{k=0}^{\infty} \epsilon^k \rho_f^k(x,y,t) \quad \text{for } x \in \Omega,\ y \in \mathcal{Q}_f,\ t > 0, \tag{2.4.6}$$

$$\rho_m^\epsilon(x,t) \sim \sum_{k=0}^{\infty} \epsilon^k \rho_m^k(x,y,t) \quad \text{for } x \in \Omega,\ y \in \mathcal{Q}_m,\ t > 0. \tag{2.4.7}$$

Also, assume explicitly that the ρ_f^k are $\mathcal{Q}_f$-periodic in y.

If we substitute the series (2.4.6)–(2.4.7) into the equations of our model (2.4.1/ϵ)–(2.4.4./ϵ), expand the gradient according to (2.4.5), and collect terms with like powers

of ϵ, then from (2.4.1/ϵ) we obtain three equations for the ϵ^{-2}, ϵ^{-1}, and ϵ^0 terms when $x \in \Omega$, $y \in \mathcal{Q}_f$, and $t > 0$:

$$(2.4.1/\text{-}2) \qquad -\nabla_y \cdot \left[\frac{K^*}{\mu c}\nabla_y \rho_f^0\right] = 0,$$

$$(2.4.1/\text{-}1) \qquad -\nabla_y \cdot \left[\frac{K^*}{\mu c}(\nabla_y \rho_f^1 + \nabla_x \rho_f^0 - cg(\rho_f^0)^2)\right] - \nabla_x \cdot \left[\frac{K^*}{\mu c}\nabla_y \rho_f^0\right] = 0,$$

$$(2.4.1/0) \qquad \Phi^* \rho_{f,t}^0 - \nabla_y \cdot \left[\frac{K^*}{\mu c}(\nabla_y \rho_f^2 + \nabla_x \rho_f^1 - 2cg\,\rho_f^0 \rho_f^1)\right]$$
$$- \nabla_x \cdot \left[\frac{K^*}{\mu c}(\nabla_y \rho_f^1 + \nabla_x \rho_f^0 - cg(\rho_f^0)^2)\right] = q_{\text{ext}}.$$

The first equations, for ϵ^0, from (2.4.2/ϵ) and (2.4.3/ϵ) are

$$(2.4.2/0) \qquad \phi\,\rho_{m,t}^0 - \nabla_y \cdot \left[\frac{\mathbf{k}}{\mu c}(\nabla_y \rho_m^0 - cg(\rho_m^0)^2)\right] = q_{\text{ext}} \quad \text{for } x \in \Omega,\ y \in \mathcal{Q}_m,\ t > 0,$$

$$(2.4.3/0) \qquad \rho_m^0 = \rho_f^0 \quad \text{for } x \in \Omega,\ y \in \partial\mathcal{Q}_m,\ t > 0,$$

since points on $\partial\Omega_m^\epsilon$ are described globally by $x \in \Omega$ and locally by $y \in \partial\mathcal{Q}_m$. The ϵ^{-1}, ϵ^0, and ϵ^1 equations of (2.4.4/ϵ) for $x \in \Omega$, $y \in \partial\mathcal{Q}_m$, and $t > 0$ are

$$(2.4.4/\text{-}1) \qquad \left[\frac{K^*}{\mu c}\nabla_y \rho_f^0\right] \cdot \nu = 0,$$

$$(2.4.4/0) \qquad \left[\frac{K^*}{\mu c}(\nabla_y \rho_f^1 + \nabla_x \rho_f^0 - cg(\rho_f^0)^2)\right] \cdot \nu = 0,$$

$$(2.4.4/1) \qquad \left[\frac{K^*}{\mu c}(\nabla_y \rho_f^2 + \nabla_x \rho_f^1 - 2cg\,\rho_f^0 \rho_f^1)\right] \cdot \nu = \left[\frac{\mathbf{k}}{\mu c}(\nabla_y \rho_m^0 - cg(\rho_m^0)^2)\right] \cdot \nu.$$

No other equations need be considered. As $\epsilon \to 0$, $\rho_f^\epsilon \to \rho_f^0$ and $\rho_m^\epsilon \to \rho_m^0$. These limits are the "locally averaged" functions and the equations above combine to give a system in them. Equations (2.4.1/-2) and (2.4.4/-1) together form an elliptic system for ρ_f^0 in terms of the y-variable; since its solution vanishes as a function of y, it follows that

$$(2.4.8) \qquad \rho_f^0 = \rho_f^0(x,t) \quad \text{only.}$$

This corresponds to our intuition: the local average of ρ_f does not oscillate. Thus, all terms containing $\nabla_y \rho_f^0$ vanish.

Next, the equations (2.4.1/-1) and (2.4.4/0) form an elliptic system in y for ρ_f^1 that can be solved for ρ_f^1 in terms of ρ_f^0. To this end, define $\omega_j(y)$ for $j = 1,2,3$ as the $\mathcal{Q}_f$-periodic solution of

$$(2.4.9) \qquad \nabla_y^2 \omega_j = 0 \quad \text{for } y \in \mathcal{Q}_f,$$

$$(2.4.10) \qquad \nabla_y \omega_j \cdot \nu = -e_j \cdot \nu = -\nu_j \quad \text{for } y \in \partial\mathcal{Q}_m,$$

where e_j is the unit vector in the jth direction. Then, by (2.4.8),

$$\rho_f^1(x,y,t) = \sum_{j=1}^{3} \omega_j(y) \left[\frac{\partial \rho_f^0}{\partial x_j}(x,t) - c g_j (\rho_f^0)^2 \right]. \tag{2.4.11}$$

(Actually (2.4.11) holds up to an arbitrary, additive function of x and t. Since only $\nabla_y \rho_f^1$ occurs below, this ambiguity is unimportant.)

We analyze (2.4.1/0) next. Locally average it by integrating it over $\mathcal{Q}_f$ and dividing the result by $|\mathcal{Q}|$ to remove the y-variable; then

$$\begin{aligned} \frac{|\mathcal{Q}_f|}{|\mathcal{Q}|} \Phi^* \rho_{f,t}^0 - \frac{1}{|\mathcal{Q}|} \int_{\mathcal{Q}_f} \nabla_y \cdot \left[\frac{K^*}{\mu c} \left(\nabla_y \rho_f^2 + \nabla_x \rho_f^1 - 2cg \rho_f^0 \rho_f^1 \right) \right] dy \\ - \frac{1}{|\mathcal{Q}|} \int_{\mathcal{Q}_f} \nabla_x \cdot \left[\frac{K^*}{\mu c} \left(\nabla_y \rho_f^1 + \nabla_x \rho_f^0 - cg(\rho_f^0)^2 \right) \right] dy = \frac{|\mathcal{Q}_f|}{|\mathcal{Q}|} q_{\text{ext}}. \end{aligned} \tag{2.4.12}$$

Apply the divergence theorem to the first integral above, use (2.4.4/1), make a second application of the divergence theorem, and use (2.4.2/0) to see that

$$\begin{aligned} - \int_{\mathcal{Q}_f} \nabla_y \cdot \left[\frac{K^*}{\mu c} \left(\nabla_y \rho_f^2 + \nabla_x \rho_f^1 - 2cg \rho_f^0 \rho_f^1 \right) \right] dy \\ = - \int_{\partial \mathcal{Q}_f} \left[\frac{K^*}{\mu} \left(\nabla_y \rho_f^2 + \nabla_x \rho_f^1 - 2cg \rho_f^0 \rho_f^1 \right) \right] \cdot \nu \, ds(y) \\ = \int_{\partial \mathcal{Q}_m} \left[\frac{\mathbf{k}}{\mu c} \left(\nabla_y \rho_m^0 - cg(\rho_m^0)^2 \right) \right] \cdot \nu \, ds(y) \\ = \int_{\mathcal{Q}_m} \nabla_y \cdot \left[\frac{\mathbf{k}}{\mu c} \left(\nabla_y \rho_m^0 - cg(\rho_m^0)^2 \right) \right] dy \\ = \int_{\mathcal{Q}_m} \left(\phi \rho_{m,t}^0 - q_{\text{ext}} \right) dy. \end{aligned} \tag{2.4.13}$$

We have used periodicity to see that no contribution arises from the integral over $\partial \mathcal{Q}$, the outer boundary of $\mathcal{Q}_f$, and the fact that the outer normal to $\partial \mathcal{Q}_f$ is opposite to that of $\partial \mathcal{Q}_m$. Since (2.4.4/1) established the continuity of the mass flux, we have found the matrix source term. The second integral in (2.4.12) is evaluated using (2.4.11); its integrand becomes

$$\begin{aligned} \nabla_x \cdot \left[\frac{K^*}{\mu c} \left(\nabla_y \rho_f^1 + \nabla_x \rho_f^0 - cg(\rho_f^0)^2 \right) \right] \\ = \sum_{k=1}^{3} \frac{\partial}{\partial x_k} \left[\frac{K^*}{\mu c} \left(\sum_{j=1}^{3} \frac{\partial \omega_j}{\partial y_k} \left(\frac{\partial \rho_f^0}{\partial x_j} - cg_j \rho_f^0 \right) + \frac{\partial \rho_f^0}{\partial x_k} - cg_k (\rho_f^0)^2 \right) \right] \\ = \sum_{k=1}^{3} \sum_{j=1}^{3} \frac{\partial}{\partial x_k} \left[\frac{K^*}{\mu c} \left(\frac{\partial \omega_j}{\partial y_k} + \delta_{jk} \right) \left(\frac{\partial \rho_f^0}{\partial x_j} - cg_j \rho_f^0 \right) \right], \end{aligned} \tag{2.4.14}$$

where δ_{jk} is the kronecker symbol. We can now *define* the fracture permeability tensor $\mathbf{K} = \{K_{ij}\}$:

$$K_{ij} = \frac{1}{|\mathcal{Q}|}\left\{ \int_{\mathcal{Q}_f} \frac{\partial \omega_j}{\partial y_k}\, dy + |\mathcal{Q}_f|\, \delta_{ij} \right\}. \tag{2.4.15}$$

Note that $\mathbf{K}$ reflects the geometry of the fracture system through the functions ω_j.

Finally, we have the equation for ρ_f^0:

$$\Phi\, \rho^0_{f,t} - \nabla_x \cdot \left[\frac{\mathbf{K}}{\mu c} \left(\nabla_x\, \rho^0_f - cg(\rho^0_f)^2 \right) \right] = q_{\text{ext}} + q_m, \tag{2.4.16}$$

where $\Phi = |\mathcal{Q}_f|\, \Phi^* \,/|\mathcal{Q}|$ is clearly the macroscopic fracture porosity and

$$q_m = -\frac{1}{|\mathcal{Q}|} \int_{\mathcal{Q}_m} \phi\, \rho^0_{m,t}\, dy. \tag{2.4.17}$$

With (2.4.2/0) and (2.4.3/0) (and the outer boundary condition (2.2.6) and the initial conditions (2.2.7)–(2.2.8)), we have a complete model for the flow.

We should make a few brief remarks. First, the necessary requirement for physical relevance that $\mathbf{K}$ be symmetric and positive definite can be demonstrated [6]. Second, the formal arguments leading to convergence of the model as $\epsilon \longrightarrow 0$ can be made rigorous, at least if the gravity term is linearized as described in §§2.6 below. See [6] for details. The argument there gives a somewhat less physically clear picture than that given by the formalism here, but the mathematical proof confirms that the formal picture is correct.

2.5. A comparison of the two versions of the model.

The only noticeable difference between the two versions of the model is that the external source term appears in the matrix equations of the homogenized model but not in the physically defined one. This term was left out of the latter version deliberately; it is not very significant and it would be appropriate to delete it from the homogenized version.

The other differences are subtler. The physically defined version of the model has a finite number of finite-sized matrix blocks, whereas the homogenized version has an infinite number of infinitely small matrix blocks, one for each $x \in \Omega$. As a consequence, the matrix source term is defined in the former version by a finite sum; it is an integral in the latter version. This difference has no consequence in practice, as we must restrict to a finite number of blocks to approximate the solution numerically.

What should be emphasized is that the form of the equations is the same. In particular, the matrix source term is defined to be the total amount of fluid leaving the matrix blocks per unit volume. Also, the boundary value on each block is constant in space, being explicitly a local average when the block has some size and being simply the value at the point where the block is when it is infinitely small. Again, in practice, these conditions are the same.

2.6. Some mathematical properties of the model.

The single phase model is mathematically relatively simple. Further, the system of differential equations can be made linear by an approximation of the terms that contain the gravitational vector. This is frequently done, since the densities of the fluids do not change greatly in any reasonable simulation. So, let ρ_{ref} be a constant reference density, and approximate ρ^2 by

$$\rho^2 = [(\rho - \rho_{\text{ref}}) + \rho_{\text{ref}}]^2 \approx \rho_{\text{ref}}(2\rho - \rho_{\text{ref}}) \tag{2.6.1}$$

in (2.2.1), (2.2.2), and (2.2.6), and also in (2.4.2/0) and (2.4.16).

With this modification (and with (2.2.9)), it has been shown [5], [6] that there exists a unique solution ρ_f and ρ_m to the differential system of either version of the model. Moreover, the solution depends continuously on the data q_{ext}, $\rho_{\text{init},f}$, and ρ_{ref}. Thus, a small change (or error) in the data produces only a small change in the solution, as measured in appropriate Sobolev spaces.

§3. Two-phase Immiscible Flow

3.1. Introduction.

We consider saturated, two-phase, incompressible, immiscible flow, the phases being o (oil) and w (water), with densities and viscosities ρ_α and μ_α, $\alpha = o, w$, respectively. We begin by recalling the equations that govern such flow in a single porosity system. Let $s(x,t)$ denote the w-saturation, so that the o-phase has saturation $1-s$. Let $p_\alpha(x,t)$, $\alpha = o, w$, represent the pressure in the α-phase, and denote the capillary pressure between the two phases by

$$p_c(s) = p_o - p_w, \tag{3.1.1}$$

where, as usual, $p_c(s)$ is assumed to be a function of s only. With w being the wetting phase, $p_c(s)$ typically is a decreasing function of s, as shown in Figure 7. It becomes infinite as the saturation tends to the residual water saturation s_{min}, and it is zero at the residual oil saturation corresponding to $s = s_{\text{max}}$.

The presence of one phase interferes with the flow of the other. This is quantified by defining relative permeability functions $k_{r\alpha}(s)$, $\alpha = o, w$, as functions of the saturation (see Figure 8 for typical examples). Usually, $k_{rw}(s_{\text{min}}) = k_{ro}(s_{\text{max}}) = 0$. Finally, let $\mathbf{k}(x)$ be the absolute permeability, so that $\mathbf{k}k_{r\alpha}$ is the permeability of the rock to the α-phase at the point x with saturation s.

It is more convenient to work with the potentials

$$\psi_\alpha = p_\alpha - \rho_\alpha g z, \quad \alpha = o, w, \tag{3.1.2}$$

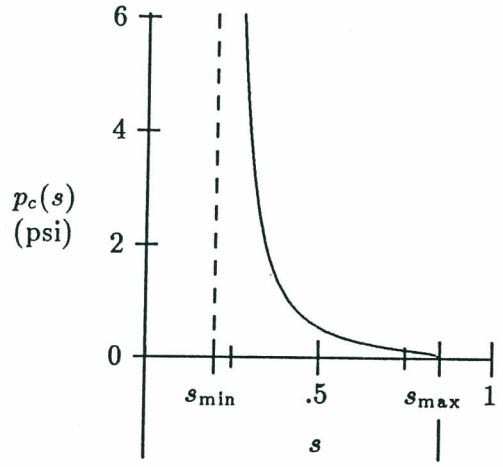

FIG. 7. A typical capillary pressure function.

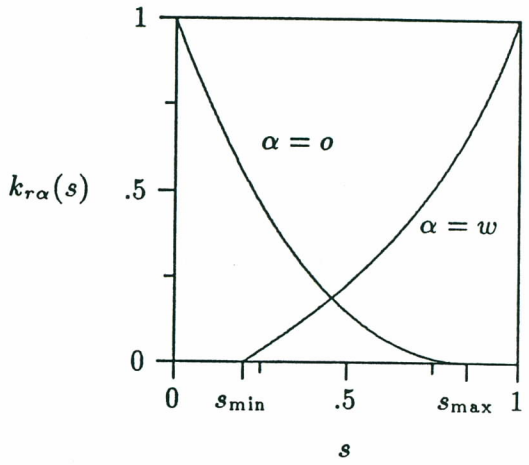

FIG. 8. Typical relative permeability functions.

than pressures; from here on g is the gravitational constant (not vector) and $z(x)$ is the depth. Darcy's law for the volumetric flow rates in two-phase flow takes the form

$$v_\alpha = -\lambda_\alpha(s)\,\nabla\psi_\alpha, \quad \alpha = o, w, \tag{3.1.3}$$

where the phase mobilities are defined by

$$\lambda_\alpha(s) = \frac{\mathbf{k}k_{r\alpha}(s)}{\mu_\alpha}, \quad \alpha = o, w. \tag{3.1.4}$$

Incompressibility and conservation of mass (or, equivalently, volume) imply that

$$\phi\, s_t + \nabla \cdot v_w = q_{\text{ext},w}, \tag{3.1.5}$$

$$-\phi\, s_t + \nabla \cdot v_o = q_{\text{ext},o}, \tag{3.1.6}$$

where $q_{\text{ext},\alpha}$ is the external volumetric α-source.

It is convenient to define a "capillary potential",

$$\psi_c = \psi_o - \psi_w = p_c(s) - (\rho_o - \rho_w)gz, \tag{3.1.7}$$

and to use it and ψ_w as the primary dependent variables. Then,

$$s = p_c^{-1}\big(\psi_c + (\rho_o - \rho_w)gz\big) \tag{3.1.8}$$

is defined from ψ_c and

$$v_o = -\lambda_o(s)\nabla(\psi_w + \psi_c). \tag{3.1.9}$$

It is frequently useful to define a total volumetric flow rate and a total mobility by

$$v = v_o + v_w = -\lambda(s)\,\nabla\psi_w - \lambda_o(s)\nabla\psi_c, \tag{3.1.10}$$

$$\lambda(s) = \lambda_w(s) + \lambda_o(s), \tag{3.1.11}$$

respectively, and to add (3.1.5) and (3.1.6) to obtain a *pressure* equation,

$$\nabla \cdot v = q_{\text{ext}}, \tag{3.1.12}$$

where $q_{\text{ext}} = q_{\text{ext},o} + q_{\text{ext},w}$ is the total external volumetric source. Then, (3.1.5) is called the *saturation* equation.

In summary, the basic equations for describing two-phase, incompressible, immiscible flow in a single porosity system are given by (3.1.3), (3.1.5), (3.1.8), and either (3.1.6) and (3.1.9) or (3.1.10)–(3.1.12).

3.2. Modeling by physical arguments.

There exists an extensive literature on the modeling of immiscible flow in naturally fractured reservoirs; among them, we cite [21], [23], [24], [31], [33], [35]. Most of these papers consider models that effectively define the matrix-fracture interaction by introducing various *ad hoc* parameters; the rest do not incorporate the matrix boundary condition in any general way. Herein we consider models [7], [8], [16], [17], [19] that treat the interaction explicitly through boundary conditions on the matrix blocks.

We denote fracture quantities by upper case letters and matrix quantities by corresponding lower case letters.

Capillary pressure and relative permeability functions are somewhat different in the fractures than in the matrix blocks. Generally, one assumes that the fractures are essentially like spaces between two parallel planes and that $S_{\min} = 0$ and $S_{\max} = 1$. Typical examples are shown in Figure 9.

There are matrix source terms $q_{m,\alpha}$, $\alpha = o, w$, for each of the phases. The saturation, pressure, and capillary equations in the fracture system can be written as

$$\Phi\, S_t - \nabla \cdot [\Lambda_w(S)\nabla\Psi_w] = q_{\text{ext},w} + q_{m,w} \quad \text{for } x \in \Omega,\ t > 0, \tag{3.2.1}$$

$$-\nabla \cdot [\Lambda(S)\nabla\Psi_w + \Lambda_o(S)\nabla\Psi_c] = q_{\text{ext}} \quad \text{for } x \in \Omega,\ t > 0, \tag{3.2.2}$$

$$S = P_c^{-1}\big(\Psi_c + (\rho_o - \rho_w)gz\big), \tag{3.2.3}$$

since incompressibility requires that $q_{m,o} + q_{m,w} = 0$. The equations on the block Ω_i are

$$\phi\, s_t - \nabla \cdot [\lambda_w(s)\nabla\psi_w] = 0 \quad \text{for } x \in \Omega_i,\ t > 0, \tag{3.2.4}$$

$$-\nabla \cdot [\lambda(s)\nabla\psi_w + \lambda_o(s)\nabla\psi_c] = 0 \quad \text{for } x \in \Omega_i,\ t > 0, \tag{3.2.5}$$

$$s = p_c^{-1}\big(\psi_c + (\rho_o - \rho_w)gz\big), \tag{3.2.6}$$

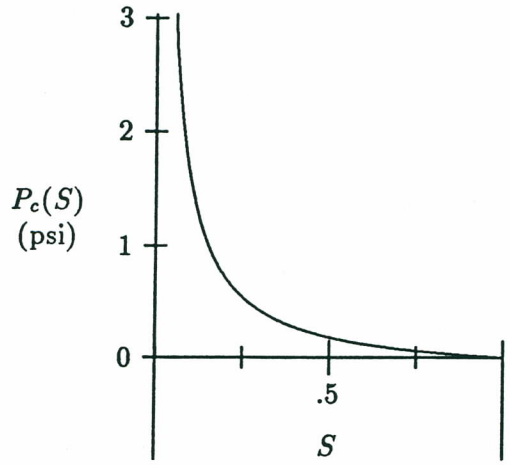

Capillary pressure.

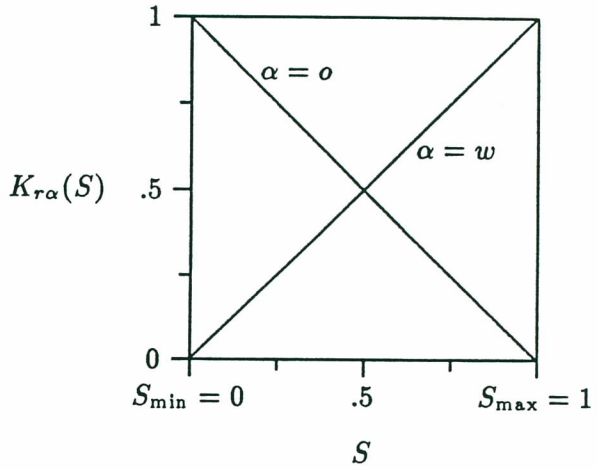

Relative permeabilities.

FIG. 9. Typical fracture functions.

where again we assume that the external sources affect the fracture system only. The boundary conditions for the matrix problems are given by requiring continuity of the potentials:

$$\psi_w(x,t) = \frac{1}{|\hat{\Omega}_i|}\int_{\hat{\Omega}_i} \Psi_w(\xi,t)\,d\xi \quad \text{for } x \in \partial\Omega_i,\ t > 0, \tag{3.2.7}$$

and

$$\psi_c(x,t) = \frac{1}{|\hat{\Omega}_i|}\int_{\hat{\Omega}_i} \Psi_c(\xi,t)\,d\xi \quad \text{for } x \in \partial\Omega_i,\ t > 0. \tag{3.2.8}$$

The matrix source terms are defined in a fashion analogous to the single phase case. The volume of the w-fluid leaving the ith block is

$$\int_{\partial\Omega_i} v_w \cdot \nu\, ds(x) = \int_{\Omega_i} \nabla \cdot v_w\, dx = -\int_{\Omega_i} \phi s_t\, dx;$$

so, let

$$q_{m,w,i}(t) = -\frac{1}{|\hat{\Omega}_i|}\int_{\Omega_i} \phi s_t\, dx \tag{3.2.9}$$

and

$$q_{m,w} = \sum_i q_{m,w,i}(t)\,\chi_i(x) \quad \text{for } x \in \Omega,\ t > 0. \tag{3.2.10}$$

We complete the model by specifying the external boundary conditions and the initial conditions for the system. For the case of no flow across the external boundary,

$$\Lambda_\alpha(s)\,\nabla\Psi_\alpha\cdot\nu=0 \quad \text{for } x\in\partial\Omega,\ t>0,\ \alpha=o,w,c. \tag{3.2.11}$$

Initial saturations (i.e., capillary potentials) must be specified:

$$\Psi_c(x,0)=\Psi_{\text{init},c}(x) \quad \text{for } x\in\Omega, \tag{3.2.12}$$

$$\psi_c(x,0)=\psi_{\text{init},c}(x) \quad \text{for } x\in\Omega_m. \tag{3.2.13}$$

To be consistent, (3.2.7), (3.2.8), and (3.2.11) should hold when $t=0$.

3.3. Modeling by homogenization.

Recall that Φ^* and K^* are the porosity and absolute permeability of the fractures on the scale of the pores, and let $\Lambda^*_\alpha(S)=K^*K_{r\alpha}(S)/\mu_\alpha$, $\alpha=o,w$, and $\Lambda^*(S)=\Lambda^*_o(S)+\Lambda^*_w(S)$. Again for simplicity, assume that the coefficients do not depend explicitly on space and time. We do *not*, however, assume them independent of saturation; this dependence is a crucial aspect of immiscible flow.

The scaled microscopic model for each $\epsilon>0$ is best defined in terms of (3.1.6) and (3.1.9), rather than (3.1.10)–(3.1.12). To exploit the natural symmetry of the equations, let $\sigma_w=1$ and $\sigma_o=-1$. Recall that $\Psi_o=\Psi_c+\Psi_w$ and $\psi_o=\psi_c+\psi_w$, and note that $S_t=\dfrac{\Psi_{c,t}}{P_c'(S)}$ and $s_t=\dfrac{\psi_{c,t}}{p_c'(s)}$. Then, in the fractures,

$$\sigma_\alpha\Phi^*\,\frac{\Psi^\epsilon_{c,t}}{P_c'(S)}-\nabla\cdot[\Lambda^*_\alpha(S)\nabla\Psi^\epsilon_\alpha]=q_{\text{ext},\alpha} \quad \text{for } x\in\Omega^\epsilon_f,\ t>0,\ \alpha=o,w, \tag{3.3.1}$$

$$S=P_c^{-1}\big(\Psi^\epsilon_c+(\rho_o-\rho_w)gz\big), \tag{3.3.2}$$

and, in the matrix,

$$\sigma_\alpha\phi\,\frac{\psi^\epsilon_{c,t}}{p_c'(s)}-\epsilon^2\nabla\cdot[\lambda_\alpha(s)\nabla\psi^\epsilon_\alpha]=q_{\text{ext},\alpha} \quad \text{for } x\in\Omega^\epsilon_m,\ t>0,\ \alpha=o,w, \tag{3.3.3}$$

$$s=p_c^{-1}\big(\psi^\epsilon_c+(\rho_o-\rho_w)gz\big). \tag{3.3.4}$$

On the matrix-fracture interface, we require continuity of the pressures and the phase volumetric fluxes; that is,

$$\psi^\epsilon_\alpha(x,t)=\Psi^\epsilon_\alpha(x,t) \quad \text{for } x\in\partial\Omega^\epsilon_m,\ t>0,\ \alpha=o,w, \tag{3.3.5}$$

$$[\Lambda^*_\alpha(S)\nabla\Psi^\epsilon_\alpha]\cdot\nu=\epsilon^2\,[\lambda_\alpha(s)\nabla\psi^\epsilon_\alpha]\cdot\nu \quad \text{for } x\in\partial\Omega^\epsilon_m,\ t>0,\ \alpha=o,w. \tag{3.3.6}$$

The correctness of the scaling follows as in the previous section. Again, were it absent, a single porosity model would result from homogenization [1], [12]. Also, the total matrix-fracture w-flow is

$$\sum_{\epsilon\text{-cells}} \int_{\epsilon\partial\mathcal{Q}_m} v_w^\epsilon \cdot \nu \, ds(x) = \sum_{\epsilon\text{-cells}} \int_{\epsilon\mathcal{Q}_m} \nabla \cdot v_w^\epsilon \, dx$$
$$= \sum_{\epsilon\text{-cells}} \int_{\epsilon\mathcal{Q}_m} \nabla \cdot [\lambda_w(s)\nabla\psi_w^\epsilon] \, dx = \sum_{\epsilon\text{-cells}} \int_{\mathcal{Q}_m} \epsilon^{-2}\nabla \cdot [\lambda_w(s)\nabla\psi_w^\epsilon]\,\epsilon^3 \, dx;$$

since there are on the order of ϵ^{-3} cells, $\lambda_w(s)$ must be scaled by ϵ^2 to preserve the flow from matrix to fractures as $\epsilon \to 0$. Similarly, $\lambda_o(s)$ (and hence $\lambda(s)$) must be scaled by ϵ^2. The definition of the potentials (3.1.2) implies that gravity has been scaled by ϵ^{-1} implicitly. If we had chosen to use the pressure variables, we would have to do this explicitly.

We again assume that every point in the reservoir is described by the general location $x \in \Omega$ and by the specific location $y \in \mathcal{Q}$ and that the solution can be expanded in power series in ϵ for $\alpha = w, c$:

$$\Psi_\alpha^\epsilon(x,t) \sim \sum_{k=0}^{\infty} \epsilon^k \Psi_\alpha^k(x,y,t), \tag{3.3.7}$$

$$\psi_\alpha^\epsilon(x,t) \sim \sum_{k=0}^{\infty} \epsilon^k \psi_\alpha^k(x,y,t). \tag{3.3.8}$$

As before, Ψ_w^k and Ψ_c^k are taken to be $\mathcal{Q}_f$-periodic in y. If we set $\Psi_o^k = \Psi_c^k + \Psi_w^k$ and $\psi_o^k = \psi_c^k + \psi_w^k$, then (3.3.7)–(3.3.8) hold with $\alpha = o$.

We shall expand saturation-dependent quantities in powers of ϵ. If θ is such a quantity, then, with "o" denoting composition of functions,

$$\begin{aligned}
\theta(s) &= \theta\left(p_c^{-1}(\psi_c^\epsilon + (\rho_o - \rho_w)gz)\right) \\
&= (\theta \circ p_c^{-1})\left(\psi_c^\epsilon + (\rho_o - \rho_w)gz\right) \\
&= (\theta \circ p_c^{-1})\left(\psi_c^0 + (\rho_o - \rho_w)gz\right) + (\theta \circ p_c^{-1})'(\sigma)(\psi_c^\epsilon - \psi_c^0) \\
&= \theta\left(p_c^{-1}(\psi_c^0 + (\rho_o - \rho_w)gz)\right) + \epsilon\hat{\theta}^1 + \epsilon^2\,\hat{\theta}^2 + \cdots
\end{aligned}$$

for some σ and $\hat{\theta}^1, \hat{\theta}^2, \ldots$. Set

$$s^0 = p_c^{-1}\left(\psi_c^0 + (\rho_o - \rho_w)gz\right), \tag{3.3.9}$$

so that

$$\theta(s) = \theta(s^0) + \sum_{k=1}^{\infty} \epsilon^k \hat{\theta}^k. \tag{3.3.10}$$

Similarly, let

$$S^0 = P_c^{-1}\big(\Psi_c^0 + (\rho_o - \rho_w)gz\big); \tag{3.3.11}$$

analogous expansions to those of (3.3.10) hold for functions of S.

Now substitute (3.3.7) and (3.3.8) into the microscopic model and expand the gradient according to (2.4.5) and the functions of saturations by (3.3.10) and collect terms by powers of ϵ. For $x \in \Omega$, $y \in \mathcal{Q}_f$, and $t > 0$, it follows from (3.3.1) for $\alpha = o, w$, that

$$-\nabla_y \cdot \big[\Lambda_\alpha^*(S^0)\nabla_y \Psi_\alpha^0\big] = 0, \tag{3.3.1/-2}$$

$$-\nabla_y \cdot \Big[\Lambda_\alpha^*(S^0)\left(\nabla_y \Psi_\alpha^1 + \nabla_x \Psi_\alpha^0\right) + \hat{\Lambda}_\alpha^{*,1}\nabla_y \Psi_\alpha^0\Big] = 0, \tag{3.3.1/-1}$$

$$\begin{aligned}\sigma_\alpha \Phi^* \frac{\Psi_{c,t}^0}{P_c'(S^0)} &- \nabla_y \cdot \big[\Lambda_\alpha^*(S^0)(\nabla_y \Psi_\alpha^2 + \nabla_x \Psi_\alpha^1) \\ &+ \hat{\Lambda}_\alpha^{*,1}(\nabla_y \Psi_\alpha^1 + \nabla_x \Psi_\alpha^0) + \hat{\Lambda}_\alpha^{*,2}\nabla_y \Psi_\alpha^0\big] \\ &- \nabla_x \cdot \big[\Lambda_\alpha^*(S^0)(\nabla_y \Psi_\alpha^1 + \nabla_x \Psi_\alpha^0) + \hat{\Lambda}_\alpha^{*,1}\nabla_y \Psi_\alpha^0\big] = q_{\text{ext},\alpha}.\end{aligned} \tag{3.3.1/0}$$

Also, from (3.3.3) and (3.3.5),

$$\sigma_\alpha \phi \frac{\psi_{c,t}^0}{p_c'(s^0)} - \nabla_y \cdot \big[\lambda_\alpha(s^0)\nabla_y \psi_\alpha^0\big] = q_{\text{ext},\alpha} \quad \text{for } x \in \Omega,\ y \in \mathcal{Q}_m,\ t > 0,\ \alpha = o, w, \tag{3.3.3/0}$$

$$\psi_\alpha^0 = \Psi_\alpha^0 \quad \text{for } x \in \Omega,\ y \in \partial\mathcal{Q}_m,\ t > 0,\ \alpha = o, w. \tag{3.3.5/0}$$

From (3.3.6) for $x \in \Omega$, $y \in \partial\mathcal{Q}_m$, $t > 0$, $\alpha = o, w$, we obtain the relations

$$\big[\Lambda_\alpha^*(S^0)\nabla_y \Psi_\alpha^0\big] \cdot \nu = 0, \tag{3.3.6/-1}$$

$$\Big[\Lambda_\alpha^*(S^0)(\nabla_y \Psi_\alpha^1 + \nabla_x \Psi_\alpha^0) + \hat{\Lambda}_\alpha^{*,1}\nabla_y \Psi_\alpha^0\Big] \cdot \nu = 0, \tag{3.3.6/0}$$

$$\begin{aligned}\Big[\Lambda_\alpha^*(S^0)(\nabla_y \Psi_\alpha^2 + \nabla_x \Psi_\alpha^1) + \hat{\Lambda}_\alpha^{*,1}(\nabla_y \Psi_\alpha^1 + \nabla_x \Psi_\alpha^0) + \hat{\Lambda}_\alpha^{*,2}\nabla_y \Psi_\alpha^0\Big] \cdot \nu \\ = \big[\lambda_\alpha(s^0)\nabla_y \psi_\alpha^0\big] \cdot \nu.\end{aligned} \tag{3.3.6/1}$$

The analysis of these equations is similar to that in §§2.4 above. First, (3.3.1/-2) and (3.3.6/-1) give homogeneous elliptic systems for the Ψ_α^0, from which we can conclude that Ψ_α^0 is independent of y:

$$\Psi_\alpha^0 = \Psi_\alpha^0(x, t) \quad \text{only, } \alpha = o, w. \tag{3.3.12}$$

This is not as easy to see as in §§2.4; the system is degenerate, since $\Lambda_w(S^0)$ is zero if $S^0 = S_{\min}$ and $\Lambda_o(S^0)$ is zero if $S^0 = S_{\max}$. Multiply (3.3.1/-2) by Ψ^0_α and integrate over $y \in \mathcal{Q}_f$; then the divergence theorem, (3.3.6/-1), and periodicity in y over $\partial\mathcal{Q}$ show that

$$-\int_{\mathcal{Q}_f} \nabla_y \cdot \left[\Lambda^*_\alpha(S^0)\nabla_y\Psi^0_\alpha\right]\Psi^0_\alpha\, dy = \int_{\mathcal{Q}_f} \Lambda^*_\alpha(S^0)|\nabla_y\Psi^0_\alpha|^2\, dx = 0.$$

Since the integrand is nonnegative, it must be zero; consequently, one of the following must hold:

i) $S^0 = S_{\min}$ and $\Psi^0_o = \Psi^0_o(x,t)$ only;

ii) $S^0 = S_{\max}$ and $\Psi^0_w = \Psi^0_w(x,t)$ only;

iii) (3.3.12) holds.

But, (3.3.11) implies that, if any two of S^0, Ψ^0_o, and Ψ^0_w are independent of y, so is the other one. Thus, (3.3.12) holds and

$$S^0 = S^0(x,t) \quad \text{only.} \tag{3.3.13}$$

Now, all terms containing $\nabla_y\Psi^0_\alpha$ or $\nabla_y S^0$ drop out.

Next, (3.3.1/-1) and (3.3.6/0) can be used to write Ψ^1_α in terms of Ψ^0_α. If $\Lambda^*_\alpha(S^0) \neq 0$,

$$\Psi^1_\alpha(x,y,t) = \sum_{j=1}^{3} \omega_j(y)\,\frac{\partial\Psi^0_\alpha}{\partial x_j}(x,t), \tag{3.3.14}$$

up to an additive function of x and t; the functions $\omega_j(y)$ are those defined in (2.4.9)–(2.4.10). Since only $\Lambda^*_\alpha(S^0)\nabla_y\Psi^1_\alpha$ is used below, the ambiguities in the value of Ψ^1_α are irrelevant.

If equation (3.3.1/0) is locally averaged, it follows that

$$\begin{aligned}\sigma_\alpha \Phi \frac{\Psi^0_{c,t}}{P'_c(S^0)} - \frac{1}{|\mathcal{Q}|}\int_{\mathcal{Q}_f} \nabla_y \cdot \left[\Lambda^*_\alpha(S^0)(\nabla_y\Psi^2_\alpha + \nabla_x\Psi^1_\alpha) + \hat{\Lambda}^{*,1}_\alpha(\nabla_y\Psi^1_\alpha + \nabla_x\Psi^0_\alpha)\right] dy \\ - \frac{1}{|\mathcal{Q}|}\int_{\mathcal{Q}_f} \nabla_x \cdot \left[\Lambda^*_\alpha(S^0)(\nabla_y\Psi^1_\alpha + \nabla_x\Psi^0_\alpha)\right] dy = \frac{|\mathcal{Q}_f|}{|\mathcal{Q}|}\, q_{\text{ext},\alpha},\end{aligned} \tag{3.3.15}$$

with the fracture porosity Φ being correctly defined earlier. Transform the first integral by use of the divergence theorem (twice) and (3.3.6/1); then,

$$\begin{aligned}&-\int_{\mathcal{Q}_f} \nabla_y \cdot \left[\Lambda^*_\alpha(S^0)(\nabla_y\Psi^2_\alpha + \nabla_x\Psi^1_\alpha) + \hat{\Lambda}^{*,1}_\alpha(\nabla_y\Psi^1_\alpha + \nabla_x\Psi^0_\alpha)\right] dy \\ &\quad = -\int_{\partial\mathcal{Q}_f} \left[\Lambda^*_\alpha(S^0)(\nabla_y\Psi^2_\alpha + \nabla_x\Psi^1_\alpha) + \hat{\Lambda}^{*,1}_\alpha(\nabla_y\Psi^1_\alpha + \nabla_x\Psi^0_\alpha)\right] \cdot \nu\, ds(y) \\ &\quad = \int_{\partial\mathcal{Q}_m} \left[\lambda_\alpha(s^0)\nabla_y\psi^0_\alpha\right] \cdot \nu\, ds(y) \\ &\quad = \int_{\mathcal{Q}_m} \nabla_y \cdot \left[\lambda_\alpha(s^0)\nabla_y\psi^0_\alpha\right] dy \\ &\quad = \int_{\mathcal{Q}_m} \left[\sigma_\alpha\phi\,\frac{\psi^0_{c,t}}{p'_c(s^0)} - q_{\text{ext},\alpha}\right] dy;\end{aligned} \tag{3.3.16}$$

again the part of the second integral above over $\partial\mathcal{Q}$ vanishes, and the outer normal to $\partial\mathcal{Q}_f$ is opposite of that to $\partial\mathcal{Q}_m$; (3.3.3/0) has been used in the last equality above.

The second integrand in (3.3.15) is simplified with (3.3.14) as follows:

$$\nabla_x \cdot \left[\Lambda_\alpha^*(S^0)\left(\nabla_y \Psi_\alpha^1 + \nabla_x \Psi_\alpha^0\right)\right] = \sum_{k=1}^{3} \frac{\partial}{\partial x_k}\left[\Lambda_\alpha^*(S^0)\left(\sum_{j=1}^{3} \frac{\partial \omega_j}{\partial y_k}\frac{\partial \Psi_\alpha^0}{\partial x_j} + \frac{\partial \Psi_\alpha^0}{\partial x_k}\right)\right] \tag{3.3.17}$$

$$= \sum_{k=1}^{3}\sum_{j=1}^{3} \frac{\partial}{\partial x_k}\left[\Lambda_\alpha^*(S^0)\left(\frac{\partial \omega_j}{\partial y_k} + \delta_{kj}\right)\frac{\partial \Psi_\alpha^0}{\partial x_j}\right].$$

Define $\mathbf{K}$ as in (2.4.15) and let

$$\Lambda_\alpha(S^0) = \frac{\mathbf{K}\, K_{r\alpha}(S^0)}{\mu_\alpha}, \quad \alpha = o, w. \tag{3.3.18}$$

Finally, set

$$q_{m,\alpha} = -\frac{\sigma_\alpha}{|\mathcal{Q}|}\int_{\mathcal{Q}_m} \phi\, \frac{\psi_{c,t}^0}{p_c'(s^0)}\, dy = -\frac{\sigma_\alpha}{|\mathcal{Q}|}\int_{\mathcal{Q}_m} \phi s_t^0\, dy \tag{3.3.19}$$

and combine (3.3.11) and (3.3.15)–(3.3.17) to obtain the equations

$$\sigma_\alpha \Phi S_t^0 - \nabla \cdot \left[\Lambda_\alpha(S^0)\nabla \Psi_\alpha^0\right] = q_{\text{ext},\alpha} + q_{m,\alpha} \quad \text{for } x \in \Omega,\ t > 0,\ \alpha = o, w. \tag{3.3.20}$$

The homogenized version consists of equations (3.3.19)–(3.3.20), (3.3.11), (3.3.3/0), (3.3.9), and (3.3.5/0), together with the initial and boundary conditions corresponding to (3.2.11)–(3.2.13). We prefer to write the model in terms of pressure and saturation equations. Add the equations (3.3.20) for $\alpha = o, w$ to obtain the pressure equation

$$-\nabla_x \cdot \left[\Lambda(S^0)\nabla_x \Psi_w^0 + \Lambda_o(S^0)\nabla_x \Psi_c^0\right] = q_{\text{ext}} \quad \text{for } x \in \Omega,\ t > 0, \tag{3.3.21}$$

where $\Lambda(S^0) = \Lambda_o(S^0) + \Lambda_w(S^0)$, to replace (3.3.20) for $\alpha = o$; the remaining equation (3.3.20) for $\alpha = w$ is the saturation equation. Similarly, replace (3.3.3/0) for $\alpha = o$ by

$$\nabla_y \cdot \left[\lambda(s^0)\nabla_y \psi_w^0 + \lambda_o(s^0)\nabla_y \psi_c^0\right] = 0 \quad \text{for } x \in \Omega,\ y \in \mathcal{Q}_m,\ t > 0, \tag{3.3.22}$$

where $\lambda(s^0) = \lambda_o(s^0) + \lambda_w(s^0)$. (We take (3.3.5/0) to hold for $\alpha = c$, also.)

The two versions of the model again have subtle differences, but none of any practical concern. The key features are reflected in both; namely, that the boundary conditions on the matrix problems are constant in space (with respect to the matrix variables) and that the matrix source term is defined as the average total flow out of the matrix blocks.

3.4. Neglecting gravity in the matrix.

When the matrix blocks are quite small, it seems reasonable for some simulations to neglect gravity in the matrix. In that case, the amount of computation required to simulate the flow can be significantly reduced, since the matrix pressure equations drop out. To see this, write the matrix equations in terms of a so-called "global pressure" variable [2], [13] defined by

$$p(x,t) = \frac{1}{2}(p_o + p_w) + \frac{1}{2}\int_0^{p_c(s)} \left(\frac{\lambda_o - \lambda_w}{\lambda}\right)(p_c^{-1}(\xi))\, d\xi \tag{3.4.1}$$
$$= p_w + \int_0^{p_c(s)} \left(\frac{\lambda_o}{\lambda}\right)(p_c^{-1}(\xi))\, d\xi,$$

so that

$$\lambda(s)\nabla p = \lambda(s)\nabla p_w + \lambda_o(s)\nabla p_c. \tag{3.4.2}$$

If the gravity terms are deleted in the matrix equations, matrix potentials are the same as matrix pressures, so that $\lambda(s)\nabla p$ is the total volumetric flow rate v (see (3.1.10)), and (3.2.5) becomes

$$\nabla \cdot (\lambda(s)\nabla p) = 0. \tag{3.4.3}$$

The boundary conditions (3.2.7)–(3.2.8) state that the pressures p_w and p_c are constant over $\partial\Omega_i$ for each i; consequently, the same is true of p. Hence, (3.4.3) is an elliptic problem with constant boundary values, so that p is this constant. Then (3.4.2) implies that

$$\lambda_w(s)\nabla p_w = -\frac{\lambda_w(s)\lambda_o(s)}{\lambda(s)}\nabla p_c, \tag{3.4.4}$$

and (3.2.4) can be rewritten in terms of s to obtain

$$\phi s_t - \nabla \cdot \left[\frac{\lambda_w(s)\lambda_o(s)}{\lambda(s)} p_c'(s)\nabla s\right] = 0 \quad \text{for } x \in \Omega_i,\ t > 0. \tag{3.4.5}$$

For emphasis, we record the boundary condition below:

$$s(x,t) = p_c^{-1}\left(\frac{1}{|\hat{\Omega}_i|}\int_{\hat{\Omega}_i} \Psi_c(\xi,t)\, d\xi + (\rho_w - \rho_o)gz\right) \quad \text{for } x \in \partial\Omega_i,\ t > 0. \tag{3.4.6}$$

These two equations and a setting of the initial saturations replace the matrix equations of the previous model.

This model can be derived from homogenization theory by not compensating gravity, so that the matrix gravity terms tend to zero with ϵ.

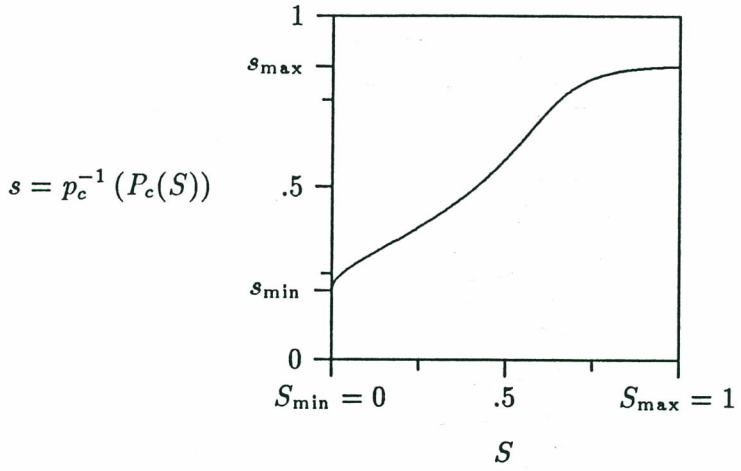

FIG. 10. A typical matrix-fracture capillary pressure relation.

3.5. A limit model.

Sometimes the fracturing is sufficiently extensive that the matrix blocks can be considered to be small enough that the fluid pressures throughout a block can be assumed in equilibrium with those in the surrounding fractures; thus, the time taken by matrix fluids to flow to the surfaces of the blocks is completely neglected. In this case the dual-porosity model can be treated as a single porosity model derivable as a simple (*not* homogenization) limit of the model of the previous subsection as the fracture spacing $\epsilon \to 0$. The validity of the limit model is not limited to fractures having the regular geometric form assumed in the models discussed so far; the size alone of the blocks is the determining factor.

As $\epsilon \to 0$, the boundary conditions (3.4.6) dominate the differential equations (3.4.5) in a block, and (3.4.6) holds in the limit on the block located at each $x \in \Omega$:

$$s(x,t) = p_c^{-1}\big(\Psi_c(x,t) + (\rho_w - \rho_o)gz\big) \quad \text{for } x \in \Omega,\ t > 0, \tag{3.5.1}$$

where we use Lebesgue's theorem on the differentiation of the integral [32] to see that, for fixed $x \in \epsilon\hat{\Omega}_i$,

$$\lim_{\epsilon \to 0} \frac{1}{|\epsilon\hat{\Omega}_i|} \int_{\epsilon\hat{\Omega}_i} \Psi_c(\xi,t)\, d\xi = \Psi_c(x,t).$$

Thus, the entire matrix problem is replaced by (3.4.6). A typical example of this very important relation is given in Figure 10. The matrix source term (3.2.9)–(3.2.10) becomes

$$\begin{aligned} q_{m,w}(x,t) &= -\lim_{\epsilon \to 0} \sum_i \left(\frac{1}{|\epsilon\hat{\Omega}_i|} \int_{\epsilon\Omega_i} \phi s_t(\xi,t)\, d\xi \right) \chi_i(x) \\ &= -\left(\frac{|\mathcal{Q}_m|}{|\mathcal{Q}|}\phi \right) s_t(x,t) \quad \text{for } x \in \Omega,\ t > 0, \end{aligned} \tag{3.5.2}$$

again by Lebesgue's theorem.

Then, (3.2.1) reduces to

$$\Phi S_t + \hat{\phi} s_t - \nabla \cdot [\Lambda_w(S) \nabla \Psi_w] = q_{\text{ext},w} \quad \text{for } x \in \Omega,\ t > 0, \tag{3.5.3}$$

with

$$\hat{\phi} = \frac{|\mathcal{Q}_m|}{|\mathcal{Q}|}\phi. \tag{3.5.4}$$

This model can be interpreted as a single porosity system with a saturation-dependent porosity for computational purposes; however, physically there remains a block associated with each point x.

§4. Some Discretization Techniques

4.1. General remarks.

Finite difference procedures for approximating the solutions to the models for single-phase or two-phase flow will be discussed, with emphasis placed on solving the matrix equations independently of the fracture equations. This is important practically, for, if only one matrix block per fracture node were employed in the computational model and if each matrix block were simulated using only one node, the size of the algebraic system would double over that in an unfractured reservoir simulation. If Gaussian elimination is used to solve any resulting large linear system, the number of arithmetic operations needed would be four to eight times that of the unfractured situation. Normally, there will be more than one matrix node per fracture node.

The simplest way to treat the fracture and matrix systems separately is to consider them sequentially. Solve first, say, for the state in the matrix blocks at the next time level, taking the matrix boundary values to be defined by the fracture data at the current time level. Then advance the fracture solution, using the new matrix data to define the matrix source term. Unfortunately, such a procedure is doomed to failure, since a small change in the boundary values can cause flow of a significant volume of fluid in comparison to the volume of the fractures. Consequently, it is easy to set up numerical oscillations: the matrix absorbs more fluid from the surrounding fractures on one step than can be resident there and then returns more to the fractures on the next step than their total volume. The matrix-fracture interaction must be handled *implicitly*, which normally would imply simultaneous solution. However, this interaction can be computed implicitly and separately by a particular linearization of the matrix problems to be made precise below. The final procedure requires solution of a large linear or nonlinear system, corresponding to the fracture equations, and many small linear systems, each corresponding to a matrix block approximated by one to a few dozen nodes. The fracture system involves about as many nodes as are used in simulation of an unfractured reservoir.

However the algebraic equations generated on each time step are solved, the separation procedure detailed below will lead to more efficient computation, but there is an added advantage of the separation when it is carried out on a parallel computing device, since matrix blocks interact only through the fracture system and do not directly affect each other. As a consequence, it is natural to solve the matrix problems in parallel, and little communication of data between processors is required. The (nonlinear) algebraic equations in the fractures can be treated either by domain decomposition techniques to solve the fracture equations in parallel or on a large vector processor. An additional possibility is to use a network consisting of a large vector computer and a set of smaller workstations. The fracture calculation can be performed on the large computer, and the matrix problems can be apportioned over the entire network [5], [19].

4.2. Some finite difference notation.

Discretize the time variable by choosing $t^0, t^1, t^2, \ldots, t^N$ such that $0 = t^0 < t^1 < t^2 < \cdots < t^N$ and set $\Delta t^n = t^n - t^{n-1}$ for $n = 1, 2, \ldots, N$.

We shall discretize the space variables by defining grids over Ω and over each matrix block Ω_i. In a finite difference context, it is simplest to consider Ω and each Ω_i to be rectangular parallelepipeds; more general domains can be treated by either finite difference or finite element techniques quite analogous to the finite difference methods to be described herein. Suppose that $\Omega = [0, D_1] \times [0, D_2] \times [0, D_3]$. Then, divide each D_j into N_j intervals, which for simplicity we take to be of equal size $H_j = D_j/N_j$, $j = 1, 2, 3$. Thus, the fracture grid is the lattice of points

$$\mathcal{G}_f = \{x_L : L = (L_1, L_2, L_3),\ x_L = (L_1 H_1, L_2 H_2, L_3 H_3), \text{ and } L_j = 0, 1, 2, \ldots, N_j,\ j = 1, 2, 3\}.$$

We shall assume for notational convenience that the matrix blocks are all of the same size and consider a grid defined on the representative matrix block $\mathcal{Q}_m$. Let h_j and n_j be analogous to H_j and N_j and set

$$\mathcal{G}_m = \{y_\ell : \ell = (\ell_1, \ell_2, \ell_3),\ y_\ell = (\ell_1 h_1, \ell_2 h_2, \ell_3 h_3),\ \text{and } \ell_j = 0, 1, 2, \ldots, n_j,\ j = 1, 2, 3\}.$$

Also, let

$$\overset{\circ}{\mathcal{G}}_m = \{y_\ell : \ell = (\ell_1, \ell_2, \ell_3),\ y_\ell = (\ell_1 h_1, \ell_2 h_2, \ell_3 h_3),\ \text{and } \ell_j = 1, 2, \ldots, n_j - 1,\ j = 1, 2, 3\}$$

indicate the interior nodes and $\partial\mathcal{G}_m = \mathcal{G}_m \setminus \overset{\circ}{\mathcal{G}}_m$ the boundary nodes. (In practice the matrix grid should be graded to place more nodes near the surface of the block [17]. Also, advantage should be taken of the symmetry of the solution on a matrix block to allow the solution to be computed only at necessary nodes.)

We wish to approximate the solutions to the models at the time levels t^n. A function Θ related to the the fracture system will be approximated at each point $x_L \in \mathcal{G}_f$; this approximation will be denoted by

$$\Theta_L^n \approx \Theta(x_L, t^n).$$

Each H_j will be larger than the spacing of the fracture planes. Only those blocks which sit over the points of $\mathcal{G}_f$ will enter the discretization process. For a function θ associated with the block at the point $x_L \in \mathcal{G}_f$, we denote the approximation to θ at $y_\ell \in \mathcal{G}_m$ by

$$\theta_{L,\ell}^n \approx \theta(x_{L,\ell}, t^n),$$

where $x_{L,\ell} = x_L - y_\ell$ (we assume that a top corner of the block is x_L).

Time derivatives will be discretized by backward Euler approximations and spatial derivatives by standard 7-point differences. Grid points adjacent to a given point x_L are denoted by $x_{L\pm e_j}$, where $e_1 = (1,0,0)$, $e_2 = (0,1,0)$, and $e_3 = (0,0,1)$. Points half-way between x_L and $x_{L\pm e_j}$ are denoted by $x_{L\pm\frac{1}{2}e_j}$. A similar notation will be employed for points adjacent to $x_{L,\ell}$.

4.3. Single phase flow.

The discretization of either version of the single phase model produces the same discrete model. Though it could easily be included using the linearization (2.6.1) [5], [19], gravity will be neglected both in the matrix blocks and in the fractures; moreover, the permeabilities will be taken to be scalar.

Let the spatial derivatives in (4.3.2) be approximated by a standard 7-point difference operator,

$$\nabla_{h,L,\ell} \cdot \left[\frac{k}{\mu c} \nabla_{h,L,\ell} \rho_m^n \right]$$
$$= \sum_{j=1}^{3} \frac{1}{h_j^2} \left\{ \frac{k(x_{L,\ell+\frac{1}{2}e_j})}{\mu c} \left(\rho_{m,L,\ell+e_j}^n - \rho_{m,L,\ell}^n \right) - \frac{k(x_{L,\ell-\frac{1}{2}e_j})}{\mu c} \left(\rho_{m,L,\ell}^n - \rho_{m,L,\ell-e_j}^n \right) \right\},$$

and the spatial operator in (4.3.5) analogously. The numerical algorithm will be described below in four parts:

i) **Initialization** at time t^0. For each L and ℓ, let

$$\rho_{f,L}^0 = \rho_{\text{init},f}(x_L) \quad \text{and} \quad \rho_{m,L,\ell}^0 = \rho_{\text{init},m}(x_{L,\ell}). \tag{4.3.1}$$

ii) **A time step in the matrix system.** For each L, ℓ, and $n \geq 1$,

$$\phi(x_{L,\ell}) \frac{\rho_{m,L,\ell}^n - \rho_{m,L,\ell}^{n-1}}{\Delta t^n} - \nabla_{h,L,\ell} \cdot \left[\frac{k}{\mu c} \nabla_{h,L,\ell} \rho_m^n \right] = 0 \quad \text{if } y_\ell \in \mathring{\mathcal{G}}_m, \tag{4.3.2}$$

$$\rho_{m,L,\ell}^n = \rho_{f,L}^n \quad \text{if } y_\ell \in \partial\mathcal{G}_m. \tag{4.3.3}$$

iii) **The matrix source term.** For each L and $n \geq 1$,

$$q^n_{m,L} = -\frac{1}{|\mathcal{Q}|} \sum_{\ell} \phi(x_{L,\ell}) \frac{\rho^n_{m,L,\ell} - \rho^{n-1}_{m,L,\ell}}{\Delta t^n} h_1 h_2 h_3. \tag{4.3.4}$$

iv) **A time step in the fracture system.** For each L and $n \geq 1$,

$$\Phi(x_L) \frac{\rho^n_{f,L} - \rho^{n-1}_{f,L}}{\Delta t^n} - \nabla_{h,L} \cdot \left[\frac{K}{\mu c} \nabla_{h,L} \rho^n_f \right] = q_{\text{ext}}(x_L, t^n) + q^n_{m,L}, \tag{4.3.5}$$

where $\rho^n_{f,L\pm e_j}$ is defined outside of $\mathcal{G}_f$ by reflection:

$$\rho^n_{f,L\pm e_j} = \rho^n_{f,L\mp e_j} \quad \text{for } x_{L\pm e_j} \notin \mathcal{G}_f. \tag{4.3.6}$$

The algorithm is completely implicit, and (4.3.3) as stated requires the simultaneous solution of ii)–iv). This can be rectified by changing the way in which it is implemented. The key idea is to recognize that (4.3.2) is linear in $\rho^n_{m,L,\ell}$ and can be solved by finding any particular solution of (4.3.2) without requiring satisfaction of (4.3.3) and adding a solution to the problem not containing the term $\rho^{n-1}_{m,L,\ell}$ but satisfying proper boundary values. The simplest way to do this is to solve for $\bar{\rho}^n_{m,L,\ell}$ such that

$$\phi(x_{L,\ell}) \frac{\bar{\rho}^n_{m,L,\ell} - \rho^{n-1}_{m,L,\ell}}{\Delta t^n} - \nabla_{h,L,\ell} \cdot \left[\frac{k}{\mu c} \nabla_{h,L,\ell} \bar{\rho}^n_m \right] = 0 \quad \text{if } y_\ell \in \mathring{\mathcal{G}}_m, \tag{4.3.7}$$

$$\rho^n_{m,L,\ell} = \rho^{n-1}_{f,L} \quad \text{if } y_\ell \in \partial\mathcal{G}_m, \tag{4.3.8}$$

and then to solve for $\breve{\rho}^n_{m,L,\ell}$ satisfying

$$\phi(x_{L,\ell}) \frac{\breve{\rho}^n_{m,L,\ell}}{\Delta t^n} - \nabla_{h,L,\ell} \cdot \left[\frac{k}{\mu c} \nabla_{h,L,\ell} \breve{\rho}^n_m \right] = 0 \quad \text{if } y_\ell \in \mathring{\mathcal{G}}_m, \tag{4.3.9}$$

$$\breve{\rho}^n_{m,L,\ell} = 1 \quad \text{if } y_\ell \in \partial\mathcal{G}_m. \tag{4.3.10}$$

Both of these problems can be solved without knowing $\rho^n_{f,L}$. Clearly,

$$\rho^n_{m,L,\ell} = \bar{\rho}^n_{m,L,\ell} + (\rho^n_{f,L} - \rho^{n-1}_{f,L}) \breve{\rho}^n_{m,L,\ell}; \tag{4.3.11}$$

however, $\rho^n_{m,L,\ell}$ cannot be evaluated until $\rho^n_{f,L}$ is obtained from iv).

Step iii) can be implemented so as to define $q^n_{m,L}$ implicitly in terms of $\rho^n_{f,L}$:

$$\begin{aligned} q^n_{m,L} = &- \frac{1}{|\mathcal{Q}|} \sum_{\ell} \phi(x_{L,\ell}) \frac{\bar{\rho}^n_{m,L,\ell} - \rho^{n-1}_{m,L,\ell}}{\Delta t^n} h_1 h_2 h_3 \\ &- \frac{\rho^n_{f,L} - \rho^{n-1}_{f,L}}{\Delta t^n} \frac{1}{|\mathcal{Q}|} \sum_{\ell} \phi(x_{L,\ell}) \breve{\rho}^n_{m,L,\ell} h_1 h_2 h_3. \end{aligned} \tag{4.3.12}$$

Now, $\rho^n_{f,L}$ can be found from iv), and the matrix solution can be updated using (4.3.11). The time step is finished. (Note that in this *linear* problem it is necessary to find $\breve{\rho}^n_{m,L,\ell}$ only once and not on each time step; the last sum in (4.3.12) need be evaluated just once, as well.)

The modified algorithm can be understood in physical terms. The problem (4.3.7)–(4.3.8) determines the flow of matrix fluid that results when a fracture system response is temporarily suspended; that is, when the boundary values on $\partial\mathcal{G}_m$ remain unchanged during the time step. The next relations, (4.3.9)–(4.4.10), determine the matrix flow that results from a unit change in the fracture density. The proper multiple of the latter solution added to the former is the complete solution to (4.3.2)–(4.3.3), as given in (4.3.11).

A finite element version of this algorithm appears in [5] and [19]. It was also shown in [5] that the solutions of the finite element scheme converge at the optimal rate as the Δt^n's and the grid spacings on $\mathcal{G}_f$ and $\mathcal{G}_m$ tend to zero to the solution of the differential model.

4.4. Immiscible flow.

The discretization of the model of §§3.2 and §§3.3 leads to an algorithm that is noticeably more complicated than the one above; however, the main ideas are quite similar. The matrix equations will be completely linearized, but *not* the fracture equations. A Newton iteration will be used to solve the nonlinear equations of the discretized fracture system; the discrete matrix system is directly solvable. The five parts of the algorithm again uncouple the calculations related to the matrix blocks from those of the fracture calculation:

i) **Initialization.** For each L and l,

$$\Psi^0_{c,L} = \Psi_{\text{init},c}(x_L), \tag{4.4.1}$$

$$\psi^0_{c,L,\ell} = \psi_{\text{init},c,L,\ell}(x_{L,\ell}), \tag{4.4.2}$$

$$S^0_L = P_c^{-1}\left(\Psi^0_{c,L} + (\rho_o - \rho_w)g\, z(x_L)\right), \tag{4.4.3}$$

$$s^0_{L,\ell} = p_c^{-1}\left(\psi^0_{c,L,\ell} + (\rho_o - \rho_w)g\, z(x_{L,\ell})\right). \tag{4.4.4}$$

The initial water potentials can be determined by solving (4.4.22) and (4.4.29) below. The Newton procedure will require an initial guess at the solution, so that it is convenient that $\Psi^0_{w,L}$ be found; the initial matrix water potential is of little interest.

ii) **Matrix system.** For each L, ℓ, and for $n \geq 1$, find $\{\bar{\psi}^n_{c,L,\ell}, \bar{\psi}^n_{w,L,\ell}\}$ by solving

$$\phi(x_{L,\ell})\,\frac{\bar{\psi}^n_{c,L,\ell} - \psi^{n-1}_{c,L,\ell}}{p_c'(s^{n-1})\Delta t^n} - \nabla_{h,L,\ell}\cdot\left[\lambda_w(s^{n-1})\nabla_{h,L,\ell}\,\bar{\psi}^n_w\right] = 0 \quad \text{if } y_\ell \in \mathring{\mathcal{G}}_m, \tag{4.4.5}$$

$$-\nabla_{h,L,\ell}\cdot\left[\lambda(s^{n-1})\nabla_{h,L,\ell}\,\bar{\psi}^n_w + \lambda_o(s^{n-1})\nabla_{h,L,\ell}\,\bar{\psi}^n_c\right] = 0 \quad \text{if } y_\ell \in \mathring{\mathcal{G}}_m, \tag{4.4.6}$$

$$\bar{\psi}^n_{c,L,\ell} = \Psi^{n-1}_{c,L} \quad \text{if } y_\ell \in \partial\mathcal{G}_m, \tag{4.4.7}$$

$$\bar{\psi}^n_{w,L,\ell} = \Psi^{n-1}_{w,L} \quad \text{if } y_\ell \in \partial\mathcal{G}_m, \tag{4.4.8}$$

and determine $\{\breve{\psi}^n_{c,L,\ell},\ \breve{\psi}^n_{w,L,\ell}\}$ and $\{\hat{\psi}^n_{c,L,\ell},\ \hat{\psi}^n_{w,L,\ell}\}$ by solving

$$\phi(x_{L,\ell})\,\frac{\breve{\psi}^n_{c,L,\ell}}{p_c'(s^{n-1})\Delta t^n} - \nabla_{h,L,\ell}\cdot\left[\lambda_w(s^{n-1})\nabla_{h,L,\ell}\,\breve{\psi}^n_w\right] = 0 \quad \text{if } y_\ell \in \mathring{\mathcal{G}}_m, \tag{4.4.9}$$

$$-\nabla_{h,L,\ell}\cdot\left[\lambda(s^{n-1})\nabla_{h,L,\ell}\,\breve{\psi}^n_w + \lambda_o(s^{n-1})\nabla_{h,L,\ell}\,\breve{\psi}^n_c\right] = 0 \quad \text{if } y_\ell \in \mathring{\mathcal{G}}_m, \tag{4.4.10}$$

$$\breve{\psi}^n_{c,L,\ell} = 1 \quad \text{if } y_\ell \in \partial\mathcal{G}_m, \tag{4.4.11}$$

$$\breve{\psi}^n_{w,L,\ell} = 0 \quad \text{if } y_\ell \in \partial\mathcal{G}_m, \tag{4.4.12}$$

and

$$\phi(x_{L,\ell})\,\frac{\hat{\psi}^n_{c,L,\ell}}{p_c'(s^{n-1})\Delta t^n} - \nabla_{h,L,\ell}\cdot\left[\lambda_w(s^{n-1})\nabla_{h,L,\ell}\,\hat{\psi}^n_w\right] = 0 \quad \text{if } y_\ell \in \mathring{\mathcal{G}}_m, \tag{4.4.13}$$

$$-\nabla_{h,L,\ell}\cdot\left[\lambda(s^{n-1})\nabla_{h,L,\ell}\,\hat{\psi}^n_w + \lambda_o(s^{n-1})\nabla_{h,L,\ell}\,\hat{\psi}^n_c\right] = 0 \quad \text{if } y_\ell \in \mathring{\mathcal{G}}_m, \tag{4.4.14}$$

$$\hat{\psi}^n_{c,L,\ell} = 0 \quad \text{if } y_\ell \in \partial\mathcal{G}_m, \tag{4.4.15}$$

$$\hat{\psi}^n_{w,L,\ell} = 1 \quad \text{if } y_\ell \in \partial\mathcal{G}_m, \tag{4.4.16}$$

where

$$\nabla_{h,L,\ell}\cdot\left[\lambda_\alpha(s^{n-1})\nabla_{h,L,\ell}\,\psi^n\right] = \sum_{j=1}^{3}\frac{1}{h_j^2}\left\{\lambda_\alpha\left(\frac{s^{n-1}_{L,\ell+e_j}+s^{n-1}_{L,\ell}}{2}\right)(\psi^n_{L,\ell+e_j}-\psi^n_{L,\ell})\right. \tag{4.4.17}$$
$$\left. -\lambda_\alpha\left(\frac{s^{n-1}_{L,\ell}+s^{n-1}_{L,\ell-e_j}}{2}\right)(\psi^n_{L,\ell}-\psi^n_{L,\ell-e_j})\right\},$$

Note that these equations are indeed linear, since the mobilities and p_c' are evaluated at the previous time level. The matrix potentials $\psi^n_{c,L,\ell}$ and $\psi^n_{w,L,\ell}$ are defined below in (4.4.25)–(4.4.26); they satisfy the expected equations, namely (4.4.28)–(4.4.31). Equations (4.4.5)–(4.4.8) define a particular solution to the linear equations, while (4.4.9)–(4.4.12) and (4.4.13)–(4.4.16) give solutions to the homogeneous problem which describe unit changes in the boundary conditions.

iii) **The matrix source term.** For each L and $n \geq 1$,

$$\tilde{\psi}^n_{w,L,\ell} = \bar{\psi}^n_{w,L,\ell} + \left(\Psi^n_{c,L} - \Psi^{n-1}_{c,L}\right)\breve{\psi}^n_{w,L,\ell} + \left(\Psi^n_{w,L} - \Psi^{n-1}_{w,L}\right)\hat{\psi}^n_{w,L,\ell}, \tag{4.4.18}$$

$$\tilde{s}^n_{L,\ell} = p_c^{-1}\left(\tilde{\psi}^n_{w,L,\ell} + (\rho_o - \rho_w)gz(x_{L,\ell})\right), \tag{4.4.19}$$

$$q^n_{m,w,L} = -\frac{1}{|\mathcal{Q}|}\sum_\ell \phi(x_{L,\ell})\,\frac{\tilde{s}^n_{L,\ell} - s^{n-1}_{L,\ell}}{\Delta t^n}\,h_1h_2h_3. \tag{4.4.20}$$

The quantity $q^n_{m,w,L}$ is given implicitly in terms of the fracture potentials at the nth time level; however, in view of (4.4.26) and (4.4.27) below, (4.4.20) is clearly a discretization of (3.2.9).

iv) **Fracture system.** (This is the most critical system to solve well.) For each L and $n \geq 1$, solve the following nonlinear system of equations for $\Psi^n_{c,L}$, $\Psi^n_{w,L}$, S^n_L and $q^n_{m,w,L}$:

$$\Phi(x_L)\frac{S^n_L - S^{n-1}_L}{\Delta t^n} - \sum_{j=1}^{3}\frac{1}{H_j^2}\left\{\Lambda^n_{w,L,j}\left(\Psi^n_{w,L+e_j} - \Psi^n_{w,L}\right) - \Lambda^n_{w,L-e_j,j}\left(\Psi^n_{w,L} - \Psi^n_{w,L-e_j}\right)\right\} = q_{\mathrm{ext},w}(x_L, t^n) + q^n_{m,w,L}, \tag{4.4.21}$$

$$-\sum_{j=1}^{3}\frac{1}{H_j^2}\left\{\Lambda^n_{L,j}\left(\Psi^n_{w,L+e_j} - \Psi^n_{w,L}\right) - \Lambda^n_{L-e_j,j}\left(\Psi^n_{w,L} - \Psi^n_{w,L-e_j}\right) + \Lambda^n_{o,L,j}\left(\Psi^n_{c,L+e_j} - \Psi^n_{c,L}\right) - \Lambda^n_{o,L-e_j,j}\left(\Psi^n_{c,L} - \psi^n_{c,L-e_j}\right)\right\} = q_{\mathrm{ext}}(x_L, t^n), \tag{4.4.22}$$

$$S^n_L = P_c^{-1}\left(\Psi^n_{c,L} + (\rho_o - \rho_w)gz(x_L)\right), \tag{4.4.23}$$

where again the no-flow boundary conditions (3.2.11) are imposed by reflection:

$$\Psi^n_{\alpha,L\pm e_j} = \Psi^n_{\alpha,L\mp e_j}, \quad \alpha = w, c,$$

if $x_{L\pm e_j}$ is outside the reservoir. The mobilities should be upstream weighted:

$$\Lambda^n_{\alpha,L,j} = \begin{cases} \Lambda_\alpha(S^n_{L+e_j}), & \text{if } \Psi^n_{\alpha,L} < \Psi^n_{\alpha,L+e_j}, \\ \Lambda_\alpha(S^n_L), & \text{otherwise,} \end{cases} \tag{4.4.24}$$

for $\alpha = o, w$ (where $\Psi^n_{o,L} = \Psi^n_{c,L} + \Psi^n_{w,L}$). This is intended to prevent numerical instabilities [17], [25].

Note that (4.4.18)–(4.4.24) form a completely implicit procedure for the fracture quantities and the boundary values on the blocks. As previously mentioned, a variant of Newton's method should be used to obtain the solution; this is not completely straightforward, because of sharp corners at $S_{\max}$ or $s_{\max}$ in the graphs of the capillary functions (Figures 7 and 9). Since the rate of convergence of Newton iteration is related to the value of the second derivatives, it is necessary to aid the convergence by, for example, requiring the solution Ψ_c to take at least two iterations to cross a value slightly above the critical value $\Psi_{c,L} = P_c(S_{\max}) - (\rho_o - \rho_w)gz = -(\rho_o - \rho_w)gz$ at any applicable point. It is also necessary

to recognize that $P_c'(S_{\max}) = p_c'(s_{\max}) = -\infty$ (or a large negative number in practice). See [17] for details.

v) **Matrix update.** For each L, ℓ, and $n \geq 1$, let

$$\psi^n_{c,L,\ell} = \bar{\psi}^n_{c,L,\ell} + \left(\Psi^n_{c,L,\ell} - \Psi^{n-1}_{c,L,\ell}\right) \breve{\psi}^n_{c,L,\ell} + \left(\Psi^n_{w,L,\ell} - \Psi^{n-1}_{w,L,\ell}\right) \hat{\psi}^n_{c,L,\ell}, \tag{4.4.25}$$

$$\psi^n_{w,L,\ell} = \bar{\psi}^n_{w,L,\ell} + \left(\Psi^n_{c,L,\ell} - \Psi^{n-1}_{c,L,\ell}\right) \breve{\psi}^n_{w,L,\ell} + \left(\Psi^n_{w,L,\ell} - \Psi^{n-1}_{w,L,\ell}\right) \hat{\psi}^n_{w,L,\ell}, \tag{4.4.26}$$

$$s^n_{L,\ell} = p_c^{-1}\left(\psi^n_{c,L,\ell} + (\rho_o - \rho_w) g z(x_{L,\ell})\right), \tag{4.4.27}$$

and the time step is done.

The above algorithm can be implemented sequentially. The following discrete matrix problem has been solved:

$$\phi(x_{L,\ell}) \frac{\psi^n_{c,L,\ell} - \psi^{n-1}_{c,L,\ell}}{p_c'(s^{n-1})\Delta t^n} - \nabla_{h,L,\ell} \cdot \left[\lambda_w(s^{n-1}) \nabla_{h,L,\ell} \psi^n_w\right] = 0 \quad \text{if } y_\ell \in \mathring{\mathcal{G}}_m, \tag{4.4.28}$$

$$-\nabla_{h,L,\ell} \cdot \left[\lambda(s^{n-1}) \nabla_{h,L,\ell} \psi^n_w + \lambda_o(s^{n-1}) \nabla_{h,L,\ell} \psi^n_c\right] = 0 \quad \text{if } y_\ell \in \mathring{\mathcal{G}}_m, \tag{4.4.29}$$

$$\psi^n_{c,L,\ell} = \Psi^n_{c,L} \quad \text{if } y_\ell \in \partial\mathcal{G}_m, \tag{4.4.30}$$

$$\psi^n_{w,L,\ell} = \Psi^n_{w,L} \quad \text{if } y_\ell \in \partial\mathcal{G}_m. \tag{4.4.31}$$

Assuming that the wetting fluid is the denser, it should be noted that the block associated with the fracture point x_L is interpreted to lie below x_L for imbibition and above for drainage; otherwise, fluid is trapped by the numerical simulation as P_c tends to zero. We have considered the case of imbibition.

It should be remarked that the discretization of the fracture system conserves mass, except for inexactness caused by not carrying out the Newton iteration to complete convergence. The linearized matrix problems do not; however, there is no *net* mass balance error, as any fluid that leaves the matrix is transmitted to the fracture system. There is a small error in the time at which fluid is transferred from one system to the other.

4.5. Simplified models for immiscible flow.

A similar procedure to that presented in the last subsection can be given for the models of §§3.4 and §§3.5. We describe the discretization of the model that neglects gravity in the matrix first; the limit model requires only a simple modification of this algorithm.

The initialization and fracture system steps (i.e., i) and iv)) of the previous algorithm remain unchanged; steps ii), iii), and v) become:

ii) **Matrix system.** For each L, ℓ, and $n \geq 1$, determine $\bar{s}^n_{L,\ell}$ and $\breve{s}^n_{L,\ell}$ by solving

$$\phi(x_{L,\ell}) \frac{\bar{s}^n_{L,\ell} - s^{n-1}_{L,\ell}}{\Delta t^n} - \nabla_{h,L,\ell} \cdot \left[\frac{\lambda_w(s^{n-1})\lambda_o(s^{n-1})}{\lambda(s^{n-1})} p_c'(s^{n-1}) \nabla_{h,L,\ell} \bar{s}^n\right] = 0 \quad \text{if } y_\ell \in \mathring{\mathcal{G}}_m, \tag{4.5.1}$$

$$\bar{s}^n_{L,\ell} = p_c^{-1}\left(\Psi^{n-1}_{c,L} + (\rho_o - \rho_w) g z(x_{L,\ell})\right) \quad \text{if } y_\ell \in \partial\mathcal{G}_m, \tag{4.5.2}$$

and

$$(4.5.3)\quad \phi(x_{L,\ell})\,\frac{\breve{s}^n_{L,\ell}}{\Delta t^n} - \nabla_{h,L,\ell}\cdot\left[\frac{\lambda_w(s^{n-1})\lambda_o(s^{n-1})}{\lambda(s^{n-1})}\,p_c'(s^{n-1})\nabla_{h,L,\ell}\,\breve{s}^n\right] = 0 \quad \text{if } y_\ell \in \mathring{\mathcal{G}}_m,$$

$$(4.5.4)\quad \breve{s}_{L,\ell} = 1 \quad \text{if } y_\ell \in \partial\mathcal{G}_m.$$

Here, the spatial derivatives are approximated as in (4.4.17) above.

iii) **The matrix source term.** For each L and $n \geq 1$, evaluate the matrix source term $q^n_{m,w,L}$ by (4.4.20), where now

$$(4.5.5)\quad \tilde{s}^n_{L,\ell} = \bar{s}^n_{L,\ell} + \left[p_c^{-1}\left(\Psi^n_{c,L} + (\rho_o - \rho_w)gz(x_L)\right) - p_c^{-1}\left(\Psi^{n-1}_{c,L} + (\rho_o - \rho_w)gz(x_L)\right)\right]\breve{s}^n_{L,\ell}.$$

v) **Matrix update.** The matrix saturation $s^n_{L,\ell}$ is equal to $\tilde{s}^n_{L,\ell}$ given by (4.5.5).

It should be clear that the matrix problem has solved the equations

$$(4.5.6)\quad \phi(x_{L,\ell})\,\frac{s^n_{L,\ell} - s^{n-1}_{L,\ell}}{\Delta t^n} - \nabla_{h,L,\ell}\cdot\left[\frac{\lambda_w(s^{n-1})\lambda_o(s^{n-1})}{\lambda(s^{n-1})}\,p_c'(s^{n-1})\nabla_{h,L,\ell}\,s^n\right] = 0 \quad \text{if } y_\ell \in \mathring{\mathcal{G}}_m,$$

$$(4.5.7)\quad s^n_{L,\ell} = p_c^{-1}\left(\Psi^n_{c,L} + (\rho_o - \rho_w)gz(x_L)\right) \quad \text{if } y_\ell \in \partial\mathcal{G}_m.$$

A finite element algorithm similar to the one above has been shown [8] to be convergent under the assumption that the mobilities do not degenerate to zero.

The limit model is the restriction of the above algorithm that results from not allowing any of the matrix nodes to lie inside the blocks; that is, $\mathring{\mathcal{G}}_m = \emptyset$. Then (4.5.7) holds for all matrix nodes, and a single linear system must be solved (the one of iv)).

§5. Some Computational Results

We present recovery curves for some simulations of petroleum reservoir waterflooding. Though these curves give only a gross indication of the flow of fluids within the reservoir, they are sufficient to illustrate important features of naturally fractured reservoir simulation.

In all cases, the reservoir is assumed horizontal and rectangular, with height 10 meters and length 300 meters. For computational simplicity, the reservoir is assumed to be uniform in the other direction; consequently, the fracture calculations are two-dimensional over Ω, though the matrix calculations must remain three-dimensional over $\mathcal{Q}$. Fracture porosity and permeability are assumed to be .01 and 1 darcy, respectively. The corresponding quantities for the matrix are .2 and 5 millidarcies. Initially, the reservoir contains 76% oil

(μ_o = .5cp and ρ_o = .7g/cm^3) and 24% water (μ_w = 2cp and ρ_w = 1g/cm^3). Water is injected uniformly into the reservoir along one end at a constant rate of one pore-volume every five years. Oil and water are produced at the top of the other end. The recovery curve is given as the graph of the cumulative amount of oil produced versus the cumulative amount of water injected. The residual water level in the matrix is .20, while the residual oil level is .15; hence, there is a maximum recovery of .62 pore-volumes. In our simulations, the only reservoir parameter that is varied is the size of the matrix blocks, which we take to be cubes.

For the spatial discretization, we took 40 nodes in the horizontal direction and 10 in the vertical direction over Ω. In the matrix block $\mathcal{Q}$, we took the equivalent of 16 interior nodes in the full model (§§3.2–§§3.3) simulations (four nodes on each of four horizontal planes), and we took the equivalent of 27 interior nodes in the simulations using the model that neglects gravity in the matrix (§§3.4). The time step varied from one day initially to twenty days near the end of the simulations. (Each entire simulation was for about twenty years.)

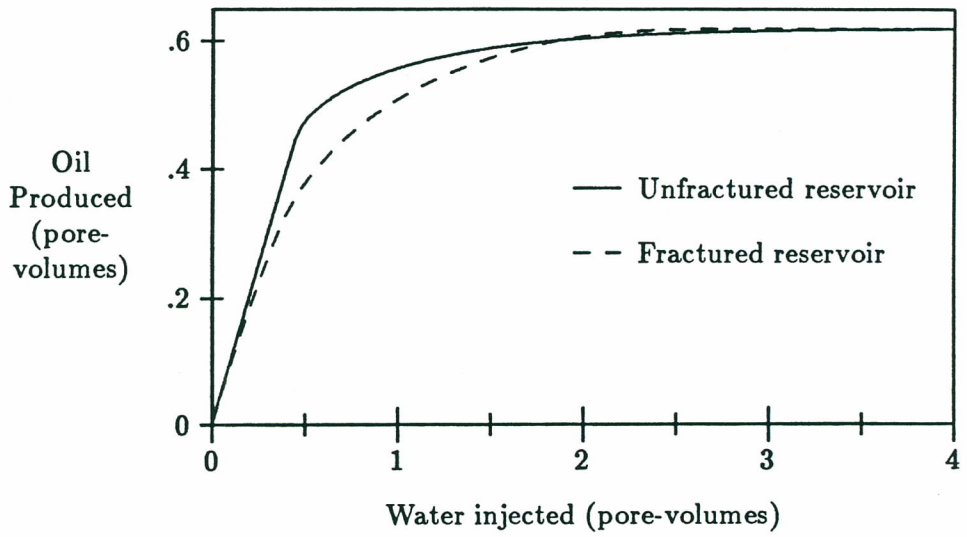

FIG. 11. A comparison of the production data for an unfractured reservoir and for a naturally fractured reservoir with matrix blocks of sidelength 200 cm.

First we compare a fractured reservoir to an unfractured one, with the unfractured one possessing the matrix properties of the fractured one, except for some minor modifications to account for the fracture space. The numerical procedure for the unfractured case is a straightforward modification (consisting of deletions) of the procedure for the fractures presented in §§4.4. The fractured reservoir has blocks of sidelength 200 cm, and the simulation is given for the full model. From Figure 11, we see that indeed there is a significant difference in response between the two reservoirs. Better sweep efficiency results in the unfractured reservoir, though it takes a much higher pressure gradient across the reservoir to obtain this recovery. The curve for the unfractured reservoir has a fairly

obvious "break-through" at about .5 pore-volumes injected, beyond which recovery drops dramatically; on the other hand, the recovery curve for the fractured reservoir varies much more gently.

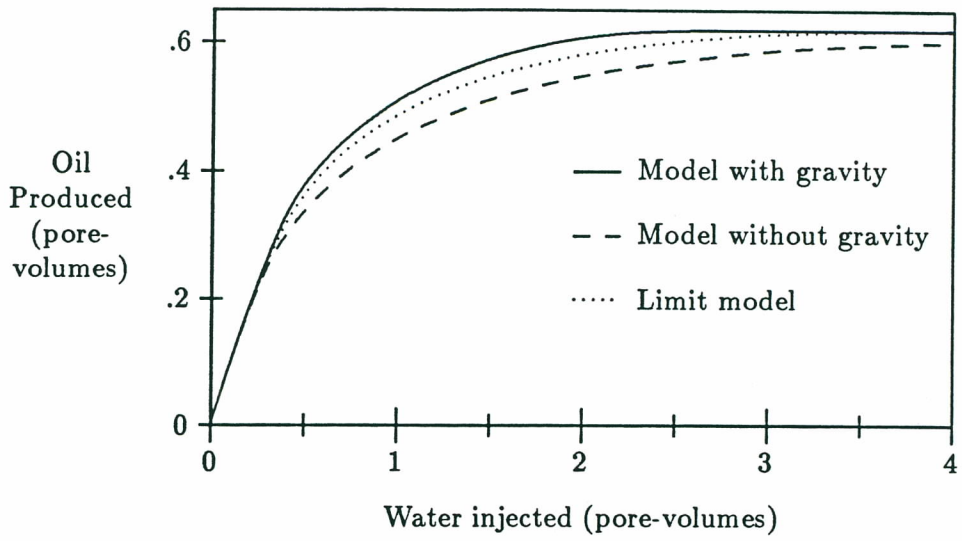

FIG. 12. A comparison of the production data for the various immiscible models for a reservoir with matrix blocks of sidelength 200 cm.

Next, we look at the three immiscible models of this presentation. As can be seen in Figure 12, these models predict significantly different recoveries. The full model predicts the greatest sweep efficiency. Surprisingly, in this series of simulations the limit model (§§3.5) seems to give a better prediction than the model which simply neglects gravity in the matrix. See [17] for additional simulations of the simplified models.

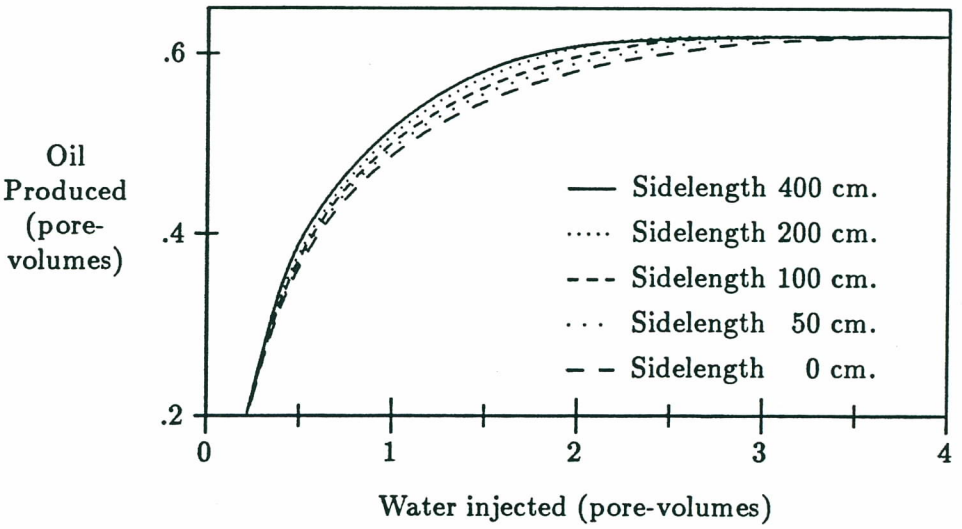

FIG. 13. The effect of matrix block size on the production data, and convergence to the limit model.

Finally, the effect of matrix block size on the full model is considered in Figure 13. Sweep efficiency increases with increasing block size. It can also be seen that, as the block size tends to zero, the recovery curves of the simulations tend to that of the limit model (where the block size is 0 cm). If we continue reducing the block size below 50 cm, the recovery curves become almost indistinguishable from that for the limit model at about 10 cm.

§6. Some Other Models

Many other dual-porosity models can be defined to incorporate various physical phenomena. We briefly mention a few of these in this section.

Miscible flows can be considered; a simple dual-porosity model for such appears in [7]. It is similar to the models presented above. A new feature is that a continuity of component mass concentration is imposed at the surfaces of each matrix block in addition to the imposition of continuity of pressure. This model is not completely satisfactory for simulating miscible displacement; the "first-order" model discussed below provides a much more realistic simulation of that physical process [4].

The immiscible waterflooding problem is sensitive to gravitational segregation of water and oil. If the matrix block height is large, it may be important to model this effect. It was incorporated somewhat crudely in the model of §3, since the block height was considered to be small (infinitely so, in the homogenized version). We assumed that at each time a potential equilibrium exists from the top to the bottom of the block at its surface. The block height can be considered to be large and only the width and depth to be small. Homogenization will produce a model in which the blocks have the original height but no width or depth. Then, the full vertical variation in the potentials is reflected in the boundary condition for the matrix problems. See [7] and [16] for more detail.

In the models treated in this presentation, the matrix boundary conditions have always imposed continuity between matrix and fracture pressures. This means that the "capillary end effect" of [27], [18], and [15] has been imposed without exception in the waterflooding models. Russell [28] has considered the possibility that flow in the fractures is sufficiently rapid that there is not enough time for equilibrium to be reached between the matrix and fracture potentials, and he has proposed replacing the strict continuity of oil pressure between the matrix and fracture systems by a "third-type" or Robin boundary condition. In our notation (see §3), this would take the form

$$-\lambda_o |p_c'(s)| \nabla s \cdot \nu = C\left(p_c(s) - \frac{1}{|\hat{\Omega}_i|} \int_{\hat{\Omega}_i} P_c(S(\xi,t))\, d\xi \right) \quad \text{for } x \in \partial\Omega_i,\ t > 0,$$

where C is some empirical constant. The effect of such a boundary condition is to permit a delay in the imbibition of water into the matrix blocks.

Finally, we mention a class of models that might be referred to as "first-order" models. These models are not strictly derived from homogenization theory, since that theory

assumes that the matrix block size tends to zero. The leading terms in these models are derived from homogenization (giving the "zeroth-order" model), but an attempt is made to take into account the actual finite size of the matrix blocks by assuming that the boundary values on each matrix block vary linearly in space at any given time, rather than being constant in space. Such a model has been considered for single-component, single-phase flow [3] and for two-component miscible flow [4].

References

[1] B. AMAZIANE AND A. BOURGEAT, *Effective behavior of two-phase flow in heterogeneous reservoir*, in Numerical Simulation in Oil Recovery, M. F. Wheeler, ed., The IMA Volumes in Mathematics and its Applications, 11, Springer-Verlag, Berlin and New York, 1988, pp. 1–22.

[2] S. N. ANTONCEV, *On the solvability of boundary value problems for degenerate two-phase porous flow equations*, Dinamika Splošnoĭ Sredy vyp., 10 (1972), pp. 28–53, (Russian).

[3] T. ARBOGAST, *The double porosity model for single phase flow in naturally fractured reservoirs*, in Numerical Simulation in Oil Recovery, M. F. Wheeler, ed., The IMA Volumes in Mathematics and its Applications, 11, Springer-Verlag, Berlin and New York, 1988, pp. 23–45.

[4] ———, *On the simulation of incompressible, miscible displacement in a naturally fractured petroleum reservoir*, R.A.I.R.O. Modél. Math. Anal. Numér, 23 (1989), to appear.

[5] ———, *Analysis of the simulation of single phase flow through a naturally fractured reservoir*, SIAM J. Numer. Anal., 26 (1989), pp. 12–29.

[6] T. ARBOGAST, J. DOUGLAS, JR. AND U. HORNUNG, *Derivation of the double porosity model of single phase flow via homogenization theory*, to appear.

[7] ———, *Modeling of naturally fractured reservoirs by formal homogenization techniques*, to appear.

[8] T. ARBOGAST, J. DOUGLAS, JR. AND J. E. SANTOS, *Two-phase immiscible flow in naturally fractured reservoirs*, in Numerical Simulation in Oil Recovery, M. F. Wheeler, ed., The IMA Volumes in Mathematics and its Applications, 11, Springer-Verlag, Berlin and New York, 1988, pp. 47–66.

[9] G. I. BARENBLATT, I. P. ZHELTOV AND I. N. KOCHINA, *Basic concepts in the theory of seepage of homogeneous liquids in fissured rocks [strata]*, Prikl. Mat. Mekh., 24 (1960), pp. 852–864. J. Appl. Math. Mech., 24 (1960), pp. 1286–1303.

[10] J. BEAR, *Dynamics of fluids in porous media*, Elsevier, New York, 1972.

[11] A. BENSOUSSAN, J. L. LIONS AND G. PAPANICOLAOU, *Asymptotic analysis for periodic structures*, North-Holland, Amsterdam, 1978.

[12] A. BOURGEAT, *Homogenization of two phase flow equations*, Proc. Symp. Pure Math., 45 (1986), pp. 157–163.

[13] G. CHAVENT, *A new formulation of diphasic incompressible flows in porous media*, in Applications of Methods of Functional Analysis to Problems in Mechanics, Lecture Notes in Mathematics 503, Springer-Verlag, Berlin and New York, 1976.

[14] G. CHAVENT AND J. JAFFRÉ, *Mathematical Models and Finite Elements for Reservoir Simulation*, North-Holland, Amsterdam, 1986.

[15] R. E. COLLINS, *Flow of Fluids Through Porous Materials*, Reinhold, New York, 1961.

[16] J. DOUGLAS, JR., *Three models for waterflooding in a naturally fractured petroleum reservoir*, to appear.

[17] J. DOUGLAS, JR., T. ARBOGAST AND P. J. PAES LEME, *Two models for the waterflooding of naturally fractured reservoirs*, in Proceedings, Tenth SPE Symposium on Reservoir Simulation, Society of Petroleum Engineers, Dallas, Texas, 1989, pp. 219–225, Paper SPE 18425.

[18] J. DOUGLAS, JR., P. M. BLAIR AND R. J. WAGNER, *Calculation of linear waterflood behavior including the effects of capillary pressure*, Trans. AIME, 213 (1958), pp. 96–104.

[19] J. DOUGLAS, JR., P. J. PAES LEME, T. ARBOGAST AND T. SCHMITT, *Simulation of flow in naturally fractured reservoirs*, in Proceedings, Ninth SPE Symposium on Reservoir Simulation, Society of Petroleum Engineers, Dallas, Texas, 1987, pp. 271–279, Paper SPE 16019.

[20] H. I. ENE, *Application of the homogenization method to transport in porous media*, this volume.

[21] J. R. GILMAN, *An efficient finite-difference method for simulating phase segregation in the matrix blocks in double-porosity reservoirs*, Soc. Petroleum Engr. J., 26 (July 1986), pp. 403–413.

[22] H. KAZEMI, *Pressure transient analysis of naturally fractured reservoirs with uniform fracture distribution*, Soc. Petroleum Engr. J., 9 (Dec. 1969), pp. 451–462.

[23] H. KAZEMI AND J. R. GILMAN, *Improved calculations for viscous and gravity displacement in matrix blocks in dual-porosity simulators*, in Proceedings, Ninth SPE Symposium on Reservoir Simulation, Society of Petroleum Engineers, Dallas, Texas, 1987, pp. 193–208, Paper SPE 16010.

[24] ———, *Improvements in simulation of naturally fractured reservoirs*, Soc. Petroleum Engr. J., 23 (Aug. 1983), pp. 695–707.

[25] D. W. PEACEMAN, *Fundamentals of Numerical Reservoir Simulation*, Elsevier, New York, 1977.

[26] S. J. PIRSON, *Performance of fractured oil reservoirs*, Bull. Amer. Assoc. Petroleum Geologists, 37 (1953), pp. 232–244.

[27] J. G. RICHARDSON, J. K. KERVER, J. A. HAFFORD AND J. S. OSOBA, *Laboratory determination of relative permeability*, Trans. AIME, 195 (1952), pp. 187–196.

[28] T. F. RUSSELL, *Formulation of a model accounting for capillary non-equilibrium in naturally fractured subsurface formations*, in Proceedings of the Fourth Wyoming Enhanced Oil Recovery Symposium, R. E. Ewing and D. Copeland, eds., University of Wyoming, Laramie, Wyoming, 1988, pp. 103–114.

[29] E. SANCHEZ-PALENCIA, *Non-homogeneous Media and Vibration Theory*, Lecture Notes in Physics, 127, Springer-Verlag, Berlin and New York, 1980.

[30] A. E. SCHEIDEGGER, *The Physics of Flow Through Porous Media*, University of Toronto Press, 1974.

[31] F. SONIER, P. SOUILLARD AND F. T. BLASKOVICH, *Numerical simulation of naturally fractured reservoirs*, Proceedings, 61st Annual Technical Conference and Exhibition of the Society of Petroleum Engineers, Dallas, Texas, 1986, Paper SPE 15627.

[32] E. M. STEIN, *Singular Integrals and Differentiability Properties of Functions*, Princeton Univ. Press, Princeton, NJ, 1970.

[33] A. de SWAAN, *Theory of waterflooding in fractured reservoirs*, Soc. Petroleum Engr. J., 18 (April 1978), pp. 117–122.

[34] ———, *Analytic solutions for determining naturally fractured reservoir properties by well testing*, Soc. Petroleum Engr. J., 16 (June 1976), pp. 117–122.

[35] L. K. THOMAS, T. N. DIXON AND R. G. PIERSON, *Fractured reservoir simulation*, Soc. Petroleum Engr. J., 23 (Feb. 1983), pp. 42–54.

[36] J. E. WARREN AND P. J. ROOT, *The behavior of naturally fractured reservoirs*, Soc. Petroleum Engr. J., 3 (Sept. 1963), pp. 245–255.